Noname manuscript No.
(will be inserted by the editor)

Hayabusa2's Superior Solar Conjunction Mission Operations

Planning and Post-operation Results

Stefania Soldini[1,2] · **Hiroshi Takeuchi**[2] · **Sho Taniguchi**[3] · **Shota Kikuchi**[2] · **Yuto Takei**[2] · **Go Ono**[2] · **Masaya Nakano**[3] · **Takafumi Ohnishi**[3] · **Takanao Saiki**[2] · **Yuichi Tsuda**[2] · **Fuyuto Terui**[2] · **Naoko Ogawa**[2] · **Yuya Mimasu**[2] · **Tadateru Takahashi**[2] · **Atsushi Fujii**[2] · **Satoru Nakazawa**[2] · **Kent Yoshikawa**[2] · **Yusuke Oki**[2] · **Chikako Hirose**[2] · **Naoki Shibata**[2] · **Hirotaka Sawada**[2] · **Tomohiro Yamaguchi**[2,*] · **Makoto Yoshikawa**[2]

Received: date / Accepted: date

Abstract In November/December 2018, the asteroid Ryugu was in the Sun shadow during the superior solar conjunction phase. As the Sun-Earth-Ryugu angle decreased under 3 degrees, the Hayabusa2 spacecraft experienced a planned 21 days of blackout in the Earth-Probe communication link. It is the first time that a spacecraft experiences solar conjunction while in hovering around a minor body. The predecessor Japanese mission, Hayabusa, experienced the solar conjunction during the transfer phase before the arrival to the asteroid Itokawa. For the safety of the spacecraft, a low energy transfer trajectory was designed in the Hill reference frame to increase its altitude from 20 km to 110 km. The trajectory was planned with the newly developed optNEAR

[1] Department of Mechanical, Materials and Aerospace Engineering
University of Liverpool, Liverpool, United Kingdom.
Tel.: +44 (0)151 795 7594
E-mail: stefania.soldini@liverpool.ac.uk

[2] Institute of Space and Astronautical Science, JAXA, Sagamihara, Japan

[3] Fujitsu Limited,Tokyo, Japan

[*] Current affiliation: Mitsubishi Electric Corporation

tool and validated with real time data. optNEAR was also used to validate JAXA's JATOPS tool for high altitude operations. As the trajectory display a "fish" like shape in the Hill's coordinates, we named it as "ayu" (sweetfish in Japanese) trajectory. In this article, the results of the conjunction operation from planning to flight data are here shown.

Keywords Superior solar conjunction · Hayabusa2 · Ryugu · Hovering satellite · Mission operations

Nomenclature

AIT	Asteroid Image Tracking
AOCS	Attitude Orbit Control System
AU	Astronomic Unit
COI	Conjunction Orbit Insertion
FD	Flight Dynamics
FOV	Field of View
GCP-NAV	Ground Control Point Navigation
goNEAR	gravitational orbits Near Earth Asteroid Regions
HGA	High Gain Antenna
HP	Home Position (20 km from the asteroid Ryugu)
HPNAV	Home Position NAVigation
HRM	Home-position Recovery Maneuver
JATOPS	JAXA Approach Trajectory OPtimizer with Stochastic constraints
OD	Orbit Determination
optNEAR	optimum trajectory Near Earth Asteroid Regions
RCS	Reaction Control System
SEP	Sun-Earth-Probe
SRP	Solar Radiation Pressure
TCM	Trajectory Control Maneuver
ToF	Time of Flight

1 Introduction

The Hayabusa2 mission is the Japanese robotic mission to the asteroid Ryugu [15]. After less than one year since arrival to Ryugu, Hayabusa2 has set a new first for Japan by successfully performing the first ever impact experiment to an asteroid on the 5^{th} of April 2019. The impact experiment was executed after completing with success another critical operation: the touchdown operation for sampling Ryugu surface (February 2018). The first touchdown was followed by a second successful touchdown at the location of the SCI's artificial crater site in July 2019. In 2018, Hayabusa2 has successfully deployed two rovers (September 2018) and a lander (October 2018) after entering in the Sun shadow in late 2018 with the start of the superior solar conjunction phase: the

subject of this paper. In November 2019, Hayabusa2 has completed its exploration phase and is now on its return journey towards the Earth. Contrary to NASA's OSIRIS-REx mission [3], the Hayabusa2 spacecraft is not orbiting the asteroid Ryugu but it is hovering at a relative distance of 20 km from its center, known as Home Position (HP) point [13]. The navigation is performed in the HP frame where the z-axis is along the Asteroid-Earth line. Hayabusa2 operations are typically around the 20 km altitude in $+z_{hp}$ known as controlled BOX-A [13]. To maintain Hayabusa2 in BOX-A, a ΔV command is send to the spacecraft every 1-2 days. When the Sun-Earth-Probe (SEP) angle decreases below 3 degrees the data noise in the Doppler measurements increase substantially [5] by making difficult to correctly send commands to the spacecraft. Previous JAXA's Hayabusa mission [17] experienced solar conjunction during the transfer phase when placed in a heliocentric orbit towards Itokawa. It is the first time that a spacecraft experiences superior solar conjunction while in a hovering phase. This condition lasted 21 days for the Hayabusa2 spacecraft by making the standard 1-2 days HP maintenance operation infeasible. As the 20 km altitude is usually artificially maintained, it was too risky to keep the spacecraft uncontrolled in proximity to the asteroid Ryugu. In order to prevent a close approach with the asteroid or an undesired escape from Ryugu's sphere of influence, the optimum trajectory Near Earth Asteroid Regions (optNEAR) tool was developed for the design of a low energy transfer trajectory for hovering satellite. The trajectory was designed in the Hill frame and due to its fish like shape was named "ayu" (Japanese sweetfish) trajectory [9]. For the case of Hayabusa2, the ayu trajectory was designed to reach an altitude of 110 km in deep conjunction (minimum SEP angle). Only two deterministic maneuvers were required with a ΔV budget of less than 1 m/s. The shooting method developed in optNEAR takes advantage of the natural dynamics of the Asteroid-Sun system, knowing that in the Hill problem the spacecraft motion is opposed by the Solar Radiation Pressure (SRP) acceleration for a fixed initial energy level. This principle was previously used by JAXA's Hiten mission [14] for the design of a recovery trajectory in the patched Sun-Earth and Earth-Moon systems [1]. The ayu trajectory aims to insert the spacecraft towards the zero velocity curves of the Hill problem (boundary of possible motion) where, the maximum altitude of 110 km is reached and, therefore, the return to a 20 km altitude can be executed in fuel-free mode (ballistic capture). As a first approximation, the conjunction trajectory is designed in the Hill frame [9] of the Sun-Asteroid system and then the solution is refined in the full-ephemeris problem. The Time of Flight (ToF) of the flown ayu conjunction trajectory is around 38 days with two deterministic ΔV deigned at the Conjunction Orbit Insertion (COI) point (Home Position before the conjunction) and at the Home Position Recovery (HRM) point (Home Position after the conjunction). Two Trajectory Correction Maneuvers (TCMs) were scheduled before and after the deep conjunction phase. The designed trajectory with the optNEAR tool was validated in real time operations and it was used for validating the JAXA's trajectory design JATOPS (JAXA Approach Trajectory

OPtimizer with Stochastic constraints) tool for high altitude operations. The result of the post-flight operations are here presented.

2 Solar Conjunction Mission Design and Operation Planning

The ayu conjunction trajectory is designed in the Hill reference frame as shown in Soldini et al [9]. The dynamics of the mother spacecraft are written in a rotating reference frame where the system is centred at the asteroid Ryugu and the Sun and the asteroid are placed along the x-axis. The Sun is in the negative x coordinates. Depending on how the initial energy of the spacecraft (state vector) is set, it is possible to distinguish regions of motion where the spacecraft dynamics are not permitted [2]. This information was used to increase the spacecraft's altitude from 20 km to a safety altitude during the deep conjunction. On 2018/12/11, the spacecraft reached the deep conjunction position located at the boundary of the permitted motion as seen in the Hill reference frame. In deep conjunction, the Sun-Earth-Probe (SEP) angle was at its minimum value of 0.4°.

The conjunction operation started and ended when the SEP angle was equal to 5° and the gravity constant of Ryugu, μ_a, was set to 30 m^3/s^2, Soldini et al [9]. Figure 1 shows the nominal conjunction trajectory as seen from the Hill reference frame, Fig. 1a, and HP reference frame, Fig. 1b. Due to the trajectory's fish-like shape in the Hill coordinates, Fig. 1b, the trajectory was named as ayu (sweetfish in Japanese) conjunction trajectory [9]. The z-axis of the HP reference frame is along the Earth-Asteroid line pointing towards the Earth. The Sun-Asteroid line belongs to the positive coordinates of the x-z plane, and the y axis is given such that the HP frame is a right-handed coordinate system.

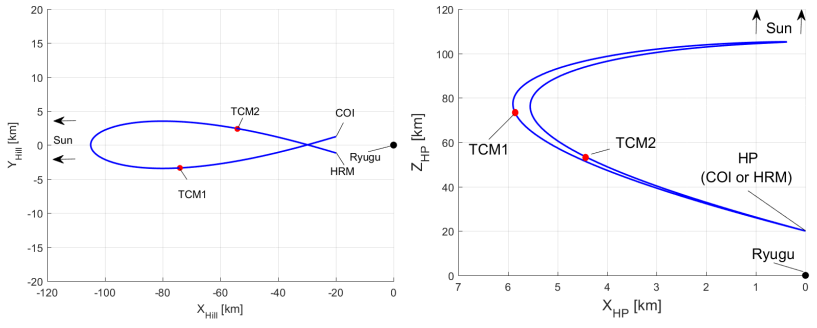

(a) Hill reference frame. (b) HP reference frame.

Fig. 1: Design solar conjunction ayu trajectory as seen in the Hill (a) and HP (b) reference frames respectively.

The ayu conjunction trajectories requires two deterministic maneuvers before and after the superior solar conjunction at the Conjunction Orbit Insertion (COI) point and the Home-position Recovery Maneuver (HRM) respectively as shown in Fig. 1 [9]. The total contribution of the two deterministic ΔV maneuver at COI and HRM computed with the optNEAR tool is of 0.2359 m/s [9]. As a result of an uncertainty analysis in the deterministic maneuvers at COI and HRM, Soldini et al. [9] concluded that at least two stochastic Trajectory Correction Maneuvers (TCMs) are required as shown in Fig. 1. The conjunction operation requires four maneuvers to be performed. The solution in the Hill reference frame is the first guess solution. The trajectory is then refined and recomputed in the full ephemeries planetary equations through the use of the NASA's SPICE toolkit, interfaced with the optNEAR tool.

Table 1 shows the epochs of the Hayabusa2's superior solar conjunction operations. The overall solar conjunction phase lasted for 37 days and the spacecraft was kept free from on ground control while in deep conjunction for 21 days. Note that on the 28^{th} of December 2018, we decided to modify the ΔV planning at HRM (last line in Tab. 1) and we merged the Home Position Keeping (HPK) maneuver for hovering position maintenance (20 km from Ryugu along z_{hp} axis) with the HRM maneuver.

Table 1: Scheduled Maneuvers for the Hayabusa2's Superior Solar Conjunction

Maneuver	Epoch [UTC]	SEP angle [°]
COI	2018/11/23	5
TCM1	2018/11/30	3
TCM2	2018/12/25	4
HRM+HPK	2018/12/29	5

In Soldini et al [9], it was demonstrated that the ayu conjunction trajectory allows a low fuel expenditure and the asteroid Ryugu is always in the Field Of View (FOV) of the Hayabusa2's wide angle navigation camera ONC-W1 (60°). Figure 2 shows the designed trajectory for $\mu_a = 32$ m^{3}s^{-2} and for a conjunction maneuver starting at a SEP angle of 6°. The left panel shows the trajectory by forward and backward integration from the deep conjunction point (-H). It was verified the geometry of the camera when the spacecraft is kept Earth-pointing ($\sim$ Sun-pointing in deep conjunction). The right panel of Fig. 2 shows the angle between the x-axis direction and the spacecraft-Ryugu line (half of the camera FOV). The asteroid is always in the FOV of the ONC-W1 camera and in some cases is within the ONC-T camera FOV (6°).

For the solar conjunction mission planning, four main phases have been defined and the epoch of the maneuvers are given in Tab. 1:

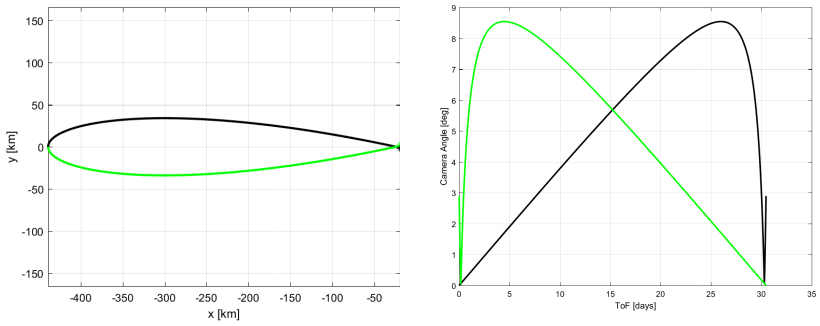

Fig. 2: The left panel shows the two arcs of the conjunction trajectory from deep conjunction to COI (green) and from deep conjunction to HRM (black). The right panel shows that the asteroid Ryugu is always in the ONC-W1 camera FOV (60°) and in some cases in the FOV of the ONC-T camera (6°).

(1) *Preparation Phase: COI (2018/11/23) - TCM1 (2018/11/30).* During the preparation phase, the spacecraft performed a 180° slew maneuver around the z_{hp}-axis to ensure the correct orientation of the 12 thrusters after the deep conjunction phase (flip of the HP frame). The COI maneuver is performed when the SEP angle is 5° and TCM1 is performed when the SEP angle is 3°.

(2) *Deep Conjunction Phase: TCM1 (2018/12/01) - TCM2 (2018/12/21).* When the spacecraft is in Deep Conjunction (SEP angle $< 3°$), the spacecraft will not perform any orbit maneuver but only attitude maintenance. Beacon operations have been done to monitor the status of the spacecraft while in deep conjunction. Radio science experiment were carried out during deep conjunction for testing the Ka-band capability of retrieving telemetry data for estimating the spacecraft's position and velocity. The spacecraft stayed in deep conjunction for 21 days with no commands send from Earth.

(3) *Recovery Phase: TCM2 (2018/12/22) - HRM (2018/12/29).* The recovery phase requires a second TCM2 maneuver when the SEP angle is 4°. The HP Recovery Maneuver (HRM) is performed when the SEP angles is 5°.

(4) *Home Position Keeping: HPK (2018/12/29).* At the HRM epoch, a ΔV for HPK maintenance was added with the scope to bring the spacecraft at 20 km altitude on the 31^{st} of December 2018.

2.1 Maneuver Operation

The conjunction orbit takes into account of the solar radiation pressure perturbation and it is designed to stay in the $+z_{hp}$ region without any deterministic maneuver between COI and HRM. The maximum distance from Ryugu was of 109 km on 2018/12/11 (deep conjunction). The COI and HRM ΔVs are of 2 cm/s in x_{hp} and 12 cm/s in y_{hp}. The maneuvers were calculated based on the results of the Orbit Determination (OD) team that made use of radiometric data and ONC-W1's Asteroid Image Tracking (AIT) data to estimate the state of the spacecraft. The AIT data were verified by using the raw ONC-W1 images. Any maneuver was supported by 2 days of navigation campaign. The minimum ΔV threshold for the Reaction Control System (RCS) is of 1 mm/s and any maneuver below 1 mm/s is cancelled. If the planned ΔV is above 10 cm/s than the maneuver is divided in main and trim ΔVs. The $\Delta \mathrm{V}_{z_{hp}}$ is measured by the 2-way Doppler, while the $\Delta \mathrm{V}_{x,y_{hp}}$ is measured by the accelerometers (ACMs). The trim ΔV is also used as a minor correction of the main ΔV during the same pass (contingency case). The Hayabusa2 spacecraft was kept Earth-pointing during the conjunction phase for radio-science purposes. The spacecraft made use of the star trackers to maintain its attitude. The attitude maneuvers were placed every three days to keep the High Gain Antenna (HGA) Earth-pointing. Every attitude slew is bellow 3°. The moving rate of the Earth direction is about 0.75 °/day and the half-band-width of the HGA is 1.2°. Note that we verified that the asteroid Ryugu is always visible with ONC-W1 (60° FOV). During the entire sequence, the SEP angle is below 2°.

Figure 3 show a schematic representation of the operation planing. Similarly to the Hayabuas2's approach phase [12], the operation planning for the solar conjunction phase can be divided in: (1) Onboard image-based optical measurements (before 7:00 UTC in Fig. 3), (2) Radio-optical hybrid navigation (between 7:00-13:00 UTC in Fig. 3), (3) Guidance (between 13:00-16:00 UTC in Fig. 3) and (4) Spacecraft operation (from 16:00 UTC in Fig. 3).

The operation planning starts two days before the maneuver planning, known as observation campaign, by downloading the telemetry from the spacecraft (1). The range-rate (RARR) and the onboard camera-based asteroid direction determination (Asteroid Image Tracking - AIT) were combined [9, 12].

To guarantee a precise relative navigation, three techniques were run in parallel (2): (a) NAV1 in Fig. 3 called HPNAV (Home Position Navigation) which is a hybrid navigation technique that combines radiometric (range and rage rate - RARR) and optical navigation (ONC-T camera) techniques. It is a method of finding the position and the speed of the spacecraft from the direction to the image center and attitude data. [12] (b) NAV2 in Fig. 3 called

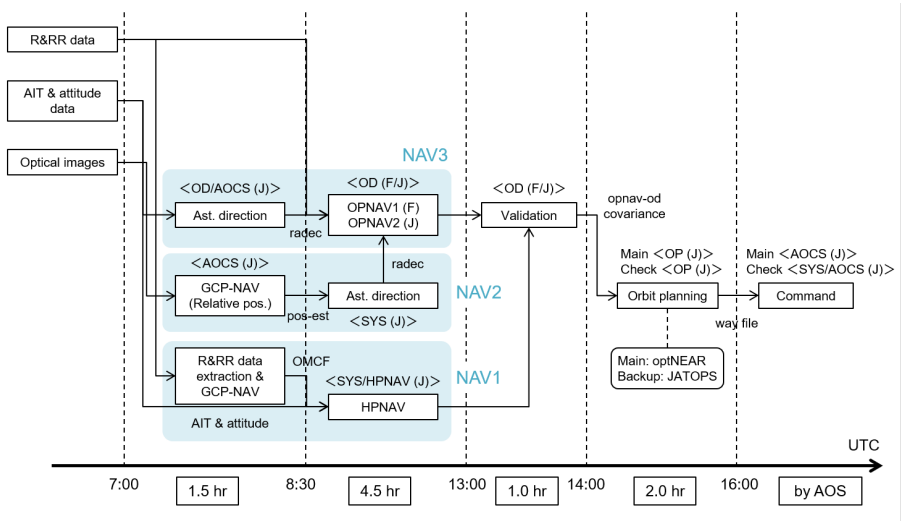

Fig. 3: Mission operation plan for each of the four scheduled conjunction maneuvers.

GCP-NAV (Ground Control Point Navigation) which is a technique of finding the position and the speed of the spacecraft by observing features on the asteroid surface [12] (c) NAV3 a full asteroid-spacecraft simultaneous orbit determination technique (Fujitsu team and JAXA team) [12].

Once the results of the navigation have been validated, the ΔV planning phase starts (3). The optNEAR tool is used as the main baseline for the ΔV planning which is the subject of this article. The JATOPS tool which was used during the approach phase [12] is now the backup solution for the solar conjunction phase. The results of the guidance are given in a way file format to be used as input to the spacecraft operation phase (4)

Finally, the spacecraft operation phase consists in transforming the way file ΔV from the HP reference frame to the spacecraft's asteroid fixed frame [9] and send the command to the spacecraft. The operation planning and the results of the mission operations are presented in this article. The mission operation process described here is followed for each of the four scheduled maneuvers at COI, TCM1, TCM2 and HRM epochs, Tab. 1.

2.2 Attitude Maintenance

The Hayabusa2 team has considered three options for the attitude maintenance of the spacecraft during deep conjunction:

1) Safe Mode (Spinning). This method is safe as the spacecraft is passively stabilised. In this mode, only range and range rate are possible. However, it consumes fuel and time to despin the spacecraft and move on to three-axis stabilisation that is its major drawback.

2) Hayabusa2 acting as a solar sail. This mode make use of 1 reaction wheel control [16,6]. The spacecraft is passively stabilised by using the Solar Radiation Pressure (SRP) torque. The passively stabilisation makes this method very safe to use. This method is inspired by JAXA's IKAROS mission [11]. The Hayabusa2 spacecraft tested this method during cruise mode [16]. However, the major disadvantage of this method is that the High Gain Antenna (HGA) can't be used when the spacecraft is in "solar sail" mode because the spacecraft would need to be kept Sun-pointing and not Earth-pointing [6].

3) Hayabusa2 is kept Earth-Pointing during deep conjunction. The spacecraft make use of the star trackers to maintain its attitude. Attitude maneuvers are required during deep conjunction which makes this method less safe than option 1) and 2). However, the HGA can be used without any difficulties.

Since the Hayabusa2 team selected the option 3) for radio-science purposes (test of the Ka-band capability in deep conjunction) [10], attitude maneuvers were placed every three days to keep the HGA Earth-pointing.

3 N-Body propagator in J2000EQ coordinates centered at Ryugu (J2000EQ-Ry): optNEAR Tool

The optNEAR tool is a trajectory optimiser that make use of N-Body propagator written in J2000 equatorial coordinates with the reference frame centered at Ryugu (J2000EQ-Ry). The optNEAR's propagator (known as goNEAR [7]) is written in python language and make use of the NASA's SPICE Toolkit package to import the ephemeris of Ryugu, all Planets, Earth, Moon and Sun. The effect of the Solar Radiation Pressure (SRP) acceleration is also taken into account. In this case, the spacecraft is considered as Earth-pointing and the flat plate model is used for the SRP acceleration [4]. The N-Body planetary equations are given by:

$$\begin{Bmatrix} \dot{X} \\ \dot{Y} \\ \dot{Z} \\ \ddot{X} \\ \ddot{Z} \end{Bmatrix} = \begin{bmatrix} \dot{X} \\ \dot{Y} \\ \dot{Z} \\ -\frac{\mu_a}{r^3}X + \sum_{j=1}^{NP_j} a_P|_{x_j} + a_{SRP}|_x \\ -\frac{\mu_a}{r^3}Y + \sum_{j=1}^{NP_j} a_P|_{y_j} + a_{SRP}|_y \\ -\frac{\mu_a}{r^3}Z + \sum_{j=1}^{NP_j} a_P|_{z_j} + a_{SRP}|_z \end{bmatrix} = \begin{bmatrix} F_1 \\ F_2 \\ F_3 \\ F_4 \\ F_5 \\ F_6 \end{bmatrix} \tag{1}$$

or in a compact way, they are:

$$\dot{\boldsymbol{X}} = \boldsymbol{F}(\boldsymbol{X}, t). \tag{2}$$

where μ_a is the gravity constant of the asteroid Ryugu (30 $\mathrm{m}^3/\mathrm{s}^2$). The 3^{rd} body acceleration is given by:

$$\boldsymbol{a}_{Pj} = -\mu_{Pj}\left(\frac{\boldsymbol{\Delta}}{\Delta^3} + \frac{\boldsymbol{d}}{d^3}\right), \tag{3}$$

with $\boldsymbol{\Delta} = \boldsymbol{r} - \boldsymbol{d}$ where $\boldsymbol{r}$ is the spacecraft's position vector from Ryugu and $\boldsymbol{d}$ is the position vector of the perturbing body (Pj) from Ryugu. Note that when the optNEAR tool calls the NASA's SPICE Toolkit, the ephemeris are downloaded from a reference frame centered in the Solar System Barycenter (SSB), therefore the vector $\boldsymbol{d}$ is given by the position vector of the planet in SSB coordinates minus the position vector of Ryugu in SSB coordinates. For a non-diffusive Earth-tracking flat surface, the SRP acceleration is:

$$\boldsymbol{a}_{SRP} = -\frac{P_0}{c}\frac{A}{m}\left(\frac{AU}{r_{ls}}\right)^2 \cos\theta\left((1-\epsilon)\frac{\boldsymbol{r}_{ls}}{r_{ls}} + 2\epsilon\cos\theta\hat{\boldsymbol{n}}\right), \tag{4}$$

where the sun-line direction ($\boldsymbol{r}_{ls}$) is given by considering the distance of the spacecraft from Ryugu minus the distance of the Sun from Ryugu. The normal vector ($\hat{\boldsymbol{n}}$) to the Hayabusa2's solar panels is kept Earth-pointing thus:

$$\hat{\boldsymbol{n}} = \frac{\boldsymbol{r}_{Earth}}{r_{Earth}}, \tag{5}$$

and

$$\cos\theta = \frac{\boldsymbol{r}_{ls}\cdot\boldsymbol{r}_{Earth}}{r_{ls}r_{Earth}} \tag{6}$$

$\boldsymbol{r}_{Earth}$ is the Ryugu-Earth distance where the vector is pointing toward the Earth. In Eq. (4), A is the spacecraft reflective area assumed as 13.276 m^2 (solar panels), the spacecraft mass, m, of 580 kg, P_0 is the solar flux of 1366 W/m^2, c is the speed of light of $2.99792458 \cdot 10^8$ m/s, ϵ is the reflectivity of the spacecraft assumed to be 0.321. Note that $\epsilon = C_r - 1$ with C_r being the reflectivity coefficient of the spacecraft ($\epsilon = 0$ complete absorption and $\epsilon = 1$ complete specular reflection). A very simple way to demonstrate the relationship between ϵ and C_r is to consider that $\rho_s + \rho_a + \rho_d = 1$ with ρ_s being the specular reflectivity coefficient, ρ_a is the absorption coefficient and ρ_d is the diffusive coefficient. If the diffusion term is neglected ($\rho_d = 0$), it is possible to write that $\rho_a = 1 - \rho_s$ and also that $C_r = 1 + \rho_s$. We renamed here ρ_s as ϵ and ρ_a as C_r.

3.1 Linearisation of the N-Body Equations (J2000EQ-Ry)

The linearised equations of Eq. (1) are:

$$\dot{\boldsymbol{x}}(t) = \boldsymbol{A}(t)\boldsymbol{x}(t) \tag{7}$$

where the matrix of the linearised equation can be derived as:

$$\boldsymbol{A} = \begin{bmatrix} 0 & 0 & 0 & 1\,0\,0 \\ 0 & 0 & 0 & 0\,1\,0 \\ 0 & 0 & 0 & 0\,0\,1 \\ \frac{\partial F_4}{\partial x} & \frac{\partial F_4}{\partial y} & \frac{\partial F_4}{\partial z} & 0\,0\,0 \\ \frac{\partial F_5}{\partial x} & \frac{\partial F_5}{\partial y} & \frac{\partial F_5}{\partial z} & 0\,0\,0 \\ \frac{\partial F_6}{\partial x} & \frac{\partial F_6}{\partial y} & \frac{\partial F_6}{\partial z} & 0\,0\,0 \end{bmatrix} \tag{8}$$

The derivatives in Eq. (8) were computed analytically and their equations are given in Appendix A. To relate a state to a specific epoch t from an initial state t_0, the state transition matrix is needed:

$$\boldsymbol{\Phi}(t, t_0) = \frac{\partial \boldsymbol{X}(t)}{\partial \boldsymbol{X}(t_0)} \tag{9}$$

that it is numerically computed as:

$$\dot{\boldsymbol{\Phi}}(t, t_0) = \boldsymbol{A}(t)\boldsymbol{\Phi}(t, t_0) \tag{10}$$

with $\boldsymbol{\Phi}(t_0, t_0) = \boldsymbol{I}$. Therefore,

$$\delta\boldsymbol{x}(t) = \boldsymbol{\Phi}(t, t_0)\delta\boldsymbol{x}(t_0). \tag{11}$$

The computation of the STM can be done by deriving the analytic expression of the linearised equations matrix $\boldsymbol{A}$ and by solving Eq. (10) numerically together with the equations of motion in Eq. (3). The derivatives in Appendix A were tested by comparing the analytical derivatives with the numerical derivatives.

4 optNAER's Single Shooting Method for the ΔV planning

The shooting methods developed in the optNEAR tool is used for the ΔV planning during the Hayabusa2's superior solar conjunction operation. The aim is to minimise the overall ΔV budget required to place the spacecraft in the ayu conjunction trajectory. The operation aims to depart from the hovering location at Home Position (HP) and return at HP after the spacecraft exit the Sun's shadow. optNEAR's shooting method aims to minimise the ΔV maneuver such that at the end of the integration of the non-linear dynamics in Eq. (1), the spacecraft returns at Home Position (HP) at the end of the

solar conjunction. To achieve high accuracy in the final error position at HP, a constrained optimisation has been used such that:

$$\min_{x,\alpha,\delta} |\Delta V| \tag{12}$$

with

$$\begin{cases} V_x = V\cos\delta\cos\alpha \\ V_y = V\cos\delta\sin\alpha \\ V_z = V\sin\delta \end{cases} \tag{13}$$

where $V = V_{max}(1+\sin x)$ and $\Delta V = \sqrt{V_x^2 + V_y^2 + V_z^2}$, subject to the following constraints:

$$\begin{array}{l} |x(t_1) - \bar{x}| - toll = 0 \\ |y(t_1) - \bar{y}| - toll = 0\,. \\ |z(t_1) - \bar{z}| - toll = 0 \end{array} \tag{14}$$

The *toll* is usually set at 0.1 meter. Note that the minimisation of the ΔV is reduced in finding three angles, α (in-plane angle), δ (out-of-plane angle) and x (e.g. $V = V_{max}$ with $x = 0°$). At t_1 after the ODE integration of Eq. (1) the final desired position of the spacecraft is to be equal to the nominal state $\bar{\boldsymbol{r}}_{HP} = [0, 0, 20\ km]$ in the HP coordinates at the end of the conjunction epoch (2018/12/29 in Tab. 1). Note that the ODE integration is performed in the J2000EQ-Ry reference frame, therefore a transformation has to be done to bring $\bar{\boldsymbol{r}}_{HP}$ in the J2000EQ-Ry coordinates ($\bar{\boldsymbol{r}}$) as shown in Soldini et al [9].

4.1 Deterministic ΔV manoeuvre at COI: Refinement of the Hill Trajectory in the N-Body Dynamics

At the beginning of the conjunction phase (COI epoch in Tab. 1), the shooting method (optNEAR tool) described makes use of the ayu conjunction trajectory designed in the Hill coordinates [9]. The ayu trajectory designed in [9] is therefore the first guess for the two-boundary value problem in the full ephemeris model (goNEAR tool [7]) were the initial (COI) and final (HRM) positions are fixed. In Fig. 4, the black line is the trajectory not optimised (goNEAR propagator), while the red trajectory is the one optimised with the optNEAR tool. The magenta point is the location of the HP at HRM (2018/12/29 in Tab. 1). Tables 2-3 show the ΔV designed at COI and HRM in the HP and J2000EQ-Ry coordinates respectively. Note that due to the mounting direction of the thrusters a ΔV margin (Tab. 2) was added to include the thrust loss in the y_{hp} direction [9]. The settings used in the optNEAR tool for the COI maneuver planning were of $V_{max} = 0.0004$ km/s. The lower and the upper boundaries of the angles were set as: x (-90°,0°), α (0°, 30°), and δ (0°, 90°)

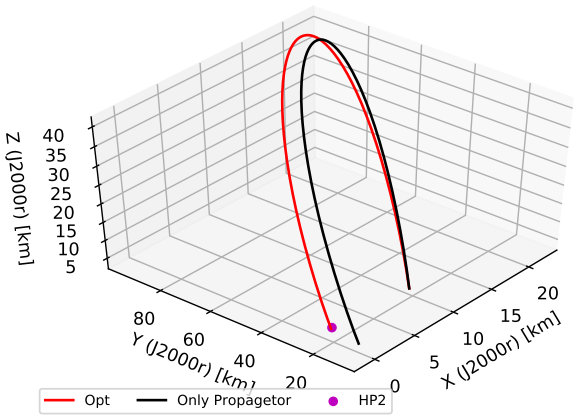

Fig. 4: Conjunction Trajectory Optimised (red) with the N-Body optimiser (optNEAR tool) and the propagated trajectory in black (goNEAR tool) as seen from Ryugu asteroid, Eq (1).

	Epoch [ET]	UTC [Date]	$\Delta V_x(HP)$ [m/s]	$\frac{\Delta V_y(HP)}{\cos(75°)}$ [m/s]	$\Delta V_z(HP)$ [m/s]
COI	596203269.18	2018/11/23 T00:00	1.891E-02	-6.0322E-03	1.175E-01
HRM	599313669.18	2018/12/29 T00:00	-1.8058E-02	1.5744E-02	-1.1549E-01
Total			3.6977E-02	2.177E-02	2.3299E-01

Table 2: ΔV in HP reference frame for the Earth-Pointing Spacecraft (μ_a = 32 m^3/s^2 and SEP = 5°).

	Epoch [ET]	UTC [Date]	$\Delta V_x(J2000)$ [m/s]	$\Delta V_y(J2000)$ [m/s]	$\Delta V_z(J2000)$ [m/s]
COI	596203269.18	2018/11/23 T00:00	3.1793E-02	1.05487E-01	4.50463E-02
HRM	599313669.18	2018/12/29 T00:00	1.4375E-02	1.07179E-01	4.4575E-02
Total			4.6168E-02	2.12666E-01	8.9621E-02

Table 3: ΔV in J2000 reference frame for the Earth-Pointing Spacecraft (μ_a = 32 m^3/s^2 and SEP = 5°).

4.2 Trajectory Correction Maneuvers: TCM1 and TCM2

After COI, every first initial state guess at the TCM epoch t_0 (time of maneuver) can be found analytically through the state transition matrix:

$$\begin{Bmatrix} \delta \boldsymbol{r}_1 \\ \delta \boldsymbol{v}_1 \end{Bmatrix} = \begin{bmatrix} \boldsymbol{\Phi}_{11} & \boldsymbol{\Phi}_{12} \\ \boldsymbol{\Phi}_{21} & \boldsymbol{\Phi}_{22} \end{bmatrix}_{t_1,t_0} \begin{Bmatrix} \delta \boldsymbol{r}_0 \\ \delta \boldsymbol{v}_0 \end{Bmatrix} \tag{15}$$

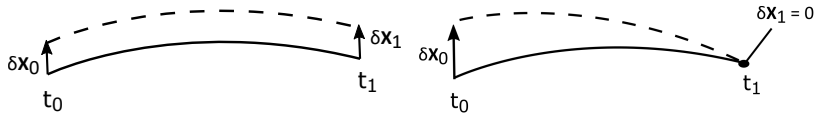

(a) State Transition Matrix. (b) Desired final position at t_1.

Fig. 5: Shooting method: reference trajectory (solid line) and perturbed trajectory (dashed line).

with the objective to bring the final position state at zero as shown in Fig. (5b) ($\delta \boldsymbol{r}_0 = 0$). The first equation in the systems of equations (15) is:

$$\boldsymbol{\Phi}_{11}(t_1, t_0)\delta \boldsymbol{r}_0 + \boldsymbol{\Phi}_{12}(t_1, t_0)\delta \boldsymbol{v}_0 = \mathbf{0} \tag{16}$$

so that

$$\delta \boldsymbol{v}_0 = -\boldsymbol{\Phi}_{12}^{-1}(t_1, t_0)\boldsymbol{\Phi}_{11}(t_1, t_0)\delta \boldsymbol{r}_0, \tag{17}$$

with $\boldsymbol{\Phi}_{11}(t_1, t_0)$ as:

$$\boldsymbol{\Phi}_{11}(t_1, t_0) = \begin{bmatrix} \Phi_{11} & \Phi_{12} & \Phi_{13} \\ \Phi_{21} & \Phi_{22} & \Phi_{23} \\ \Phi_{31} & \Phi_{32} & \Phi_{33} \end{bmatrix}_{(t_1, t_0)} \tag{18}$$

and $\boldsymbol{\Phi}_{12}(t_1, t_0)$ as:

$$\boldsymbol{\Phi}_{12}(t_1, t_0) = \begin{bmatrix} \Phi_{14} & \Phi_{15} & \Phi_{16} \\ \Phi_{24} & \Phi_{25} & \Phi_{26} \\ \Phi_{34} & \Phi_{35} & \Phi_{36} \end{bmatrix}_{(t_1, t_0)} . \tag{19}$$

The initial state is therefore:

$$\begin{cases} \boldsymbol{x}_0 = \delta \boldsymbol{x}_0 + \bar{\boldsymbol{x}}_0 \\ \boldsymbol{v}_0 = \delta \boldsymbol{v}_0 + \bar{\boldsymbol{v}}_0 \end{cases}, \tag{20}$$

and it is used as first guess for the shooting method in optNEAR. The settings used for the optNEAR tool at TCMs are:

a) TCM1 maneuver settings:
V_{max} is set to 0.002 km/s. The lower and the upper boundaries of the angles were set as: x (-90°,0°), α (0°, 30°), and δ (0°, 90°);

b) TCM2 maneuver settings:
V_{max} is set to 0.01 km/s. The lower and the upper boundaries of the angles were set as: x (-90°,0°), α (-90°, 0°), and δ (-180°, 0°).

4.3 Brake velocity maneuver at HRM and Home Position Keeping (HPK) maneuver

The planning for the ΔV maneuver at HRM includes both a brake velocity maneuver at HP on 2018/12/29 and a Home Position Keeping (HPK) maneuver for BOX-A operation maintenance until 2018/12/31. The first ΔV aims simply to stop the spacecraft at the HP arrival point (HRM). The HPK maneuver requires a design in the Hill coordinates as for the ayu conjunction trajectory. We used the same shooting method described in Soldini et al [9] but with the following initial guess: $H_0 = 25$ km (maximum altitude), $\alpha_0 = 188°$ (in-plane angle in the x-y_{hill} coordinates) and $v_{z0} = 0$ km/s (out of plane velocity). The lower and the upper boundaries of the optimum parameters are: $20 < H < 30$ km, $180° < \alpha < 270°$ and $-0.00001 < v_z < 0.00001$ km/s. Once the HPK maintenance arc has been designed in the Hill reference frame, the solution was refined in the optNEAR tool with the following settings: V_{max} is set to 0.0002 km/s. The lower and the upper boundaries of the angles were set as: x (-90°,0°), α (0°, 30°), and δ (90°, 180°). Figure 6 shows the nominal HPK arc trajectory designed with the optNEAR tool if the HRM point is in its nominal location of 20 km altitude.

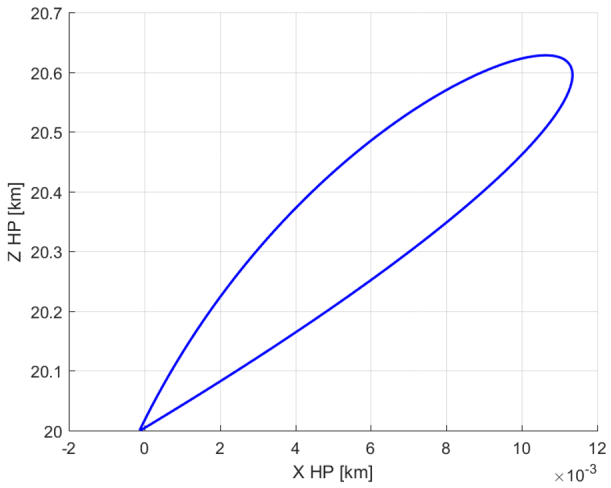

Fig. 6: Example of the HPK trajectory arc in the HP reference frame from 2018/12/29 to 2018/12/31.

5 JAXA's JATOPS Tool: the backup solution of the optNEAR tool

As part of the ΔV planning at COI, TCM1, TCM2 and HRM, we made use of the optNEAR tool as a main solution for planning the ΔV command to be executed on board the spacecraft. However, we also validated that JAXA's trajectory optimisation tool JATOPS [12] could retrieve the same solution of the optNEAR tool once the nominal states at the COI, TCM1, TCM2 and HRM epochs were computed by optNEAR. Figure 7 shows that the JATOPS tool [12] could be used for high altitude operations as the same solution designed with the optNEAR tool could be found. Therefore, our ΔV planning strategy was to use the optNEAR tool as baseline for the computation of the ΔV commands and relay on the JATOPS tool as a back-up solution. The JATOPS tool [12] was selected as back-up solution for the optNEAR tool and we confirmed the procedure to retrieve the nominal trajectory with JATOPS following:

(1) The ayu trajectory was divided in three trajectories legs from COI-TCM1 (Leg1), TCM1-TCM2 (Leg2) and TCM2-HRM (Leg3);

(2) Each leg derives a two-impulse trajectory using states derived by the optNEAR tool from the output .way file as the boundary conditions;

(3) We confirmed that the JATOPS tool was a good back-up in extreme cases when a ΔV is required to safely return back to HP;

(4) The JATOPS tool does not have the capability to derive the whole nominal ayu conjunction orbit from COI to HRM at once as the optNEAR tool in one single shooting.

6 Post Mission Operation

In this section, each of the four maneuvers performed during the solar conjunction phase are presented. The solar conjunction operation was planned as described in Section 2 and in Fig 3. For each operation planning (Fig 3), the results of the OD teams were first analysed. Once the most reliable estimate of the spacecraft's position and velocity was selected by the Flight Dynamic (FD) and Orbit Determination (OD) teams, the planning of the ΔV resulted in the delivery of the way file from the FD team to the Attitude Orbit Control System (AOCS) team. The ΔV is thus given as a sequence of commands to the spacecraft. After the ΔV is executed on board the spacecraft we measured its velocity (2-way Doppler) and acceleration (accelerates, ACMs) to estimate the actual ΔV performed. The actual and the planned ΔVs are thus compared to evaluate the performance of the operation. In case of large discrepancies

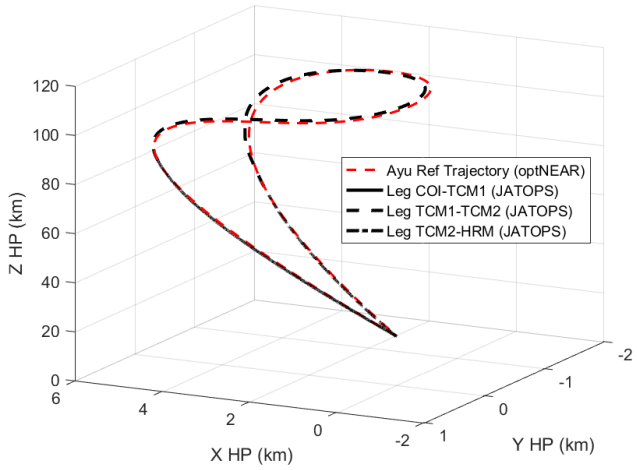

Fig. 7: The conjunction trajectory as seen from the HP frame: a comparison between the solutions obtained between the optNEAR (red line) and the JATOPS (black line) tools.

between ΔVs, it is possible to correct the maneuver within the same communication pass. At the end of the operation, the measured ΔV is used for the trajectory design of the next trajectory leg.

6.1 Conjunction Orbit Insertion (COI) Maneuver: 2018/11/23

On November, 23^{rd} 2018, the Hayabusa2 spacecraft performed the conjunction orbit insertion maneuver. The navigation and operation planning and their results are here presented. The ΔV planning started on the 22^{nd} of November after two days of data measurements. The initial downlink of the telemetry data started on the 21^{st} of November.

(a) Once the downlink of the AIT and Doppler data is concluded, the navigation teams performed an estimate of the spacecraft position and velocity. The estimates of the navigation teams at COI are shown in Tab (4). Those estimates are compared with the nominal case as shown in the table. From those estimates, the correspondent ΔVs are computed as shown in Tab (5).

In order to select the best spacecraft's state estimate among JAXA and Fujitsu solutions, the ΔVs in Tab (5) are cross evaluated with the different solutions in Tab (4). The solutions are thus propagated with goNEAR. From this analysis, the solution from Fujitsu was selected for the ΔV planning as it shown to be the most conservative solution in presence of uncer-

Table 4: Nominal state vector at COI and estimate states by Fujitsu (OPNAV1/NAV3 in Fig 3), JAXA (OPNAV2/NAV3 in Fig 3) and HPNAV (NAV1 in Fig 3).

State Estimate	x_{hp} [km]	y_{hp} [km]	z_{hp} [km]	$v_{x_{hp}}$ [mm/s]	$v_{y_{hp}}$ [mm/s]	$v_{z_{hp}}$ [mm/s]
Nominal	0	0	20	0	0	0
OD's Fujitsu	-0.0115	-0.1428	20.0692	-1.7101	1.2674	-17.9384
OD's JAXA	-0.0458	-0.1197	19.9301	-2.1938	1.4375	-17.9382
HPNAV	0.0425	-0.1217	19.7622	-1.7098	1.7039	-18.0709

Table 5: Nominal ΔV, OD's Fujitsu ΔV (OPNAV1/NAV3 in Fig 3) and OD's JAXA ΔV (OPNAV2/NAV3 in Fig 3).

State Estimate	$\Delta\mathrm{VX}_{HP}$ [cm/s]	$\Delta\mathrm{VY}_{HP}$ [cm/s]	$\Delta\mathrm{VZ}_{HP}$ [cm/s]
Nominal	1.9844	-0.1637	12.2624
OD's Fujitsu	2.1548	-0.2906	14.0497
OD's JAXA	2.2060	-0.3080	14.0625

tainties in the navigation.

(b) After having selected the estimate from the OD's Fujitsu team, the FD team prepared the ΔV planning at COI. Figure 8 shows the way file prepared on the 22^{nd} of November for the next day operation (2018/11/23). The way file is the input for the AOCS team where the ΔV is computed in body-fixed frame.

(c) The error between the planned and the actual ΔV was of 98.78% in $\Delta\mathrm{VX}_B$, 93.53% in $\Delta\mathrm{VY}_B$ and 98.53% in $\Delta\mathrm{VZ}_B$ as shown in the report of Fig 9. Due to the uncertainties in the ΔV at COI, we concluded that at least one TCM was required on 2018/11/30 before deep conjunction. We accepted errors in the ΔV lower than 4 mm/s as concluded in Soldini et al [8] where we showed that those errors resulted in few meter position error of the spacecraft. For this reason, no contingency ΔV was required at COI. We also expected that the major ΔV at TCM1 would have been in the Z component.

Figure 10 shows the planned trajectory for the selected solution (OD's Fujitsu in black). The red trajectory leg is the predicted trajectory from COI to TCM1 when the actual ΔV of the result report in Fig. 9 is used. The green trajectory is the new designed solution from TCM1 to HRM with the optNEAR tool.

```
#OBJ_SIGMA -1.000000 OPTIMIZE_INISTATE 0
#DVNUM
 4
#=============================================================================================================================|
#.     TDB              UTC            X_HP     Y_HP     Z_HP     VX_HP    VY_HP    VZ_HP     DVX_HP     DVY_HP     DVZ_HP  |
#     [day]                           [km]     [km]     [km]     [m/s]    [m/s]    [m/s]      [m/s]      [m/s]      [m/s]  |
#1------2-----------------3--------------4--------5--------6---------7--------8--------9---------10---------11---------12----|
 0  58444.875801 2018/11/22T21:00:00.0   0.0134  -0.1611  20.3121  -0.0017   0.0013  -0.0158  --------   --------   --------
 1  58445.042467 2018/11/23T01:00:00.0  -0.0115  -0.1428  20.0692   0.0198  -0.0016   0.1226    0.0215    -0.0029    0.1405
 2  58452.042467 2018/11/30T01:00:00.0   5.7393  -0.3304  76.9386   0.0010   0.0007   0.0698    0.0000     0.0000    0.0000
 3  58477.021634 2018/12/25T00:30:00.0   4.4647  -1.1012  55.7004  -0.0074   0.0022  -0.0889    0.0000     0.0000    0.0000
 4  58481.021634 2018/12/29T00:30:00.0  -0.0001   0.0001  20.0001   0.0000   0.0000   0.0000    0.0190    -0.0042    0.1205
 5  58482.021634 2018/12/30T00:30:00.0  -0.0132   0.0012  19.4549  -0.0004   0.0000  -0.0127  --------   --------   --------

#TOTAL DV
#=============================================================================================
#  dVTotal   dVx      dVy      dVz
#  [m/s]    [m/s]    [m/s]    [m/s]
#---1--------2--------3--------4-------------------------------------------------------------
   0.2642  ------   ------   ------   #SUM OF dV NORM
   0.3086  0.0405   0.0071   0.2610   #SUM OF dVx,dVy,dVz
   0.3290  0.0405   0.0275   0.2610   #SUM OF FUEL-EQUIV dVx,dVy,dVz (ATT ALGN. if dVy>0.10[m/s])
   0.3290  0.0405   0.0275   0.2610   #SUM OF FUEL-EQUIV dVx,dVy,dVz (NO ATT ALGN.)
   0.0121  0.0034   0.0090   0.0073   #Stochastic DV 2.5-sigma(99%) [m/s]
```

Fig. 8: Planned ΔV at COI in Way file format.

```
2018/11/23
=============================================================================================
TCM_ID   SC_TIME   Speed     Injection   Remarks
                   Increase  length
           [UTC]   [m/s]     [sec]
---------------------------------------------------------------------------------------------
COI_MX 01:00:33   -0.0207    -0.331      Planned Value
                  -0.020448               ACM Integral Value

COI_MZ 01:05:38    0.1000     1.503      Planned Value (TIMEREQ, 2 injections)
                   0.09453                Doppler Measuments
                   0.0933                 ACM Integral Value

COI_MY 01:10:33    0.0059     0.348      Planned Value
                   0.0054918              ACM Integral Value

COI_TZ 02:30:33    0.0405     0.620      Planned Value (Initially, 2 injections)
                   0.04597    0.701      Planned Value (COI_MZ Influence, 2 injections)
                   0.0439                Doppler Measuments
                   0.0433                ACM Integral Value
---------------------------------------------------------------------------------------------
Accuracy   DVX  0.020448/0.0207                    =   98.78%
           DVY  0.0054918/0.0059                   =   93.08%
           DVZ  (0.09453 + 0.0439)/(0.1000+0.0405) =   98.53%

           DVX  0.020448-0.0207                    =  -0.00025
           DVY  0.0054918-0.0059                   =  -0.000408
           DVZ  (0.09453 + 0.0439)-(0.1000+0.0405) =  -0.00207
=============================================================================================
```

Fig. 9: Results of the COI operation on 2018/11/23: planned and measured ΔV report.

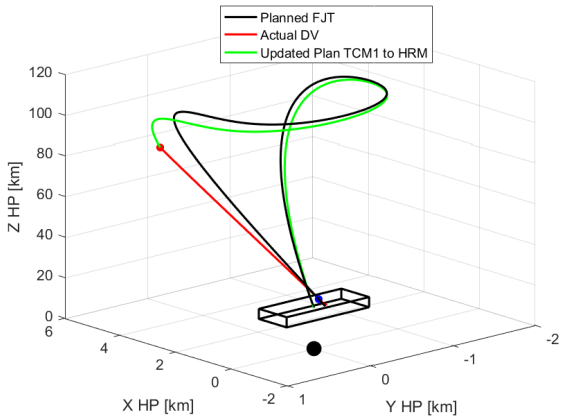

Fig. 10: Planned trajectory OD Fujitsu solution (black), actual trajectory from COI to TCM1 after COI operation (red) and new planned trajectory between TCM1 to HRM (green). The black dot represents the Ryugu coordinates. HP reference frame.

6.2 Trajectory Correction Maneuver 1 (TCM1): 2018/11/30

The first Trajectory Correction Maneuver (TCM1) was performed on November, 30^{th} 2018 before the spacecraft entered in the deep solar conjunction phase with the SEP angle equal 3°. The TCM1 allowed corrections in the trajectory after the actual operation at COI. The ΔV at TCM1 was planned on the 29^{th} of November after the initial downlink of the telemetry data on the 28^{th} of November.

(a) The estimates of the spacecraft's position and velocity on the 29^{th} of November are shown in Tab (6).
As for COI the solutions are crosschecked with the nominal case designed after the COI maneuver (green trajectory in Fig. 10). The ΔVs correspondent to the estimate solutions are shown in Tab (7). As for the COI maneuver planning, the ΔVs in Tab (7) are cross evaluated with the different solutions in Tab (6) and the solutions are propagated with goNEAR. From this analysis, the solution from JAXA was selected for the ΔV planning at TCM1.

(b) Figure 11 shows the way file prepared on the 29^{th} of November for the TCM1 operation (2018/11/30). The OD's JAXA team way file is the input for the AOCS team and the ΔV is computed in body-fixed frame.

Table 6: Nominal state vector at TCM1 and estimate states by Fujitsu (OPNAV1/NAV3 in Fig 3), JAXA (OPNAV2/NAV3 in Fig 3) and HPNAV (NAV1 in Fig 3).

State Estimate	x_{hp} [km]	y_{hp} [km]	z_{hp} [km]	$v_{x_{hp}}$ [mm/s]	$v_{y_{hp}}$ [mm/s]	$v_{z_{hp}}$ [mm/s]
Nominal	5.6589	-0.0395	75.1693	1.0321	1.1463	67.1665
OD's Fujitsu	5.6086	-0.3308	75.0280	0.5944	0.6297	67.0149
OD's JAXA	5.6395	-0.3308	74.7831	0.8847	0.6304	67.0185
HPNAV	5.8616	-0.4094	74.8879	0.9457	0.6333	68.0690

Table 7: Nominal ΔV, OD's Fujitsu ΔV (OPNAV1/NAV3 in Fig 3) and OD's JAXA ΔV (OPNAV2/NAV3 in Fig 3).

State Estimate	$\Delta\mathrm{VX}_{HP}$ [cm/s]	$\Delta\mathrm{VY}_{HP}$ [cm/s]	$\Delta\mathrm{VZ}_{HP}$ [cm/s]
Nominal	0.0230	-0.0573	0.3460
OD's Fujitsu	0.0752	0.0039	0.3674
OD's JAXA	0.0492	0.0042	0.3793

```
#OBJ_SIGMA -1.000000 OPTIMIZE_INISTATE 0
#DVNUM
 3
#=============================================================================================================================
#.     TDB                 UTC              X_HP      Y_HP      Z_HP      VX_HP     VY_HP     VZ_HP     DVX_HP     DVY_HP     DVZ_HP
#     [day]                                 [km]      [km]      [km]      [m/s]     [m/s]     [m/s]     [m/s]      [m/s]      [m/s]
#1------2-----------------3--------------4---------5---------6---------7---------8---------9---------10---------11---------12----
 0  58451.875801 2018/11/29T21:00:00.0   5.6245  -0.3396  73.8101   0.0012   0.0006   0.0681  --------   --------   --------
 1  58452.042467 2018/11/30T01:00:00.0   5.6395  -0.3308  74.7831   0.0014   0.0007   0.0708   0.0005     0.0000     0.0038
 2  58477.021634 2018/12/25T00:30:00.0   4.3881  -1.0791  55.4485  -0.0073   0.0022  -0.0882   0.0000     0.0000     0.0000
 3  58481.021634 2018/12/29T00:30:00.0  -0.0003   0.0001  19.9999   0.0000   0.0000   0.0000   0.0187    -0.0041     0.1198
 4  58482.021634 2018/12/30T00:30:00.0  -0.0134   0.0012  19.4547  -0.0004   0.0000  -0.0127  --------   --------   --------

#TOTAL DV
#=============================================================================================
#  dVTotal   dVx      dVy      dVz
#  [m/s]    [m/s]    [m/s]    [m/s]
#---1--------2--------3--------4-----------------------------------------------------------------
   0.1251  ------   ------   ------   #SUM OF dV NORM
   0.1470  0.0192   0.0042   0.1236   #SUM OF dVx,dVy,dVz
   0.1589  0.0192   0.0162   0.1236   #SUM OF FUEL-EQUIV dVx,dVy,dVz (ATT ALGN. if dVy>0.10[m/s])
   0.1589  0.0192   0.0162   0.1236   #SUM OF FUEL-EQUIV dVx,dVy,dVz (NO ATT ALGN.)
   0.0092  0.0016   0.0068   0.0059   #Stochastic DV 2.5-sigma(99%) [m/s]
```

Fig. 11: Planned ΔV at TCM1 in Way file format.

(c) In case of TCM1, the ΔVX,Y were cancelled and it resulted after 24 days in an error of 1 km in X_{HP} at TCM2 as shown in Fig 13. We registered an increase in the noise of the Doppler signal already at TCM1, Fig 12. The report in Fig. 14 shows that the error in the $\Delta\mathrm{VZ}_B$ was 99.21% resulting in a perfectly executed operation. Between TCM1 and TCM2 only pre-scheduled attitude maintenance maneuver were performed every 1-2

days. We decided to avoid the desaturation of the reaction wheels in deep conjunction to prevent errors in the planned trajectory between TCM1 and TCM2.

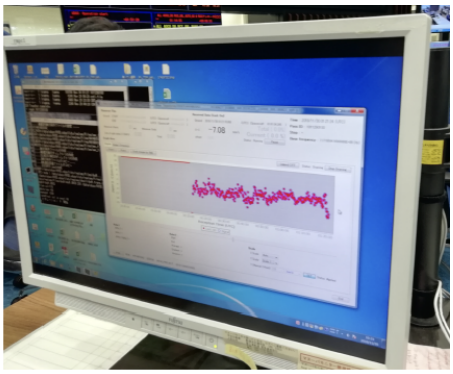

Fig. 12: Doppler signal on 2018/11/30

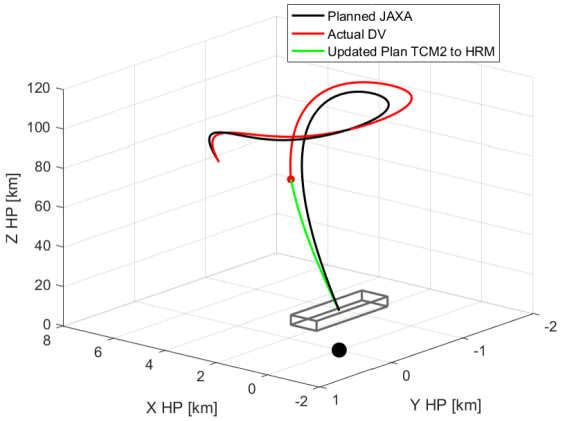

Fig. 13: Planned trajectory OD JAXA solution (black), actual trajectory from TCM1 to TCM2 after TCM1 operation (red) and new planned trajectory between TCM2 to HRM (green). The black dot represents the Ryugu coordinates. HP reference frame.

2018/11/30

TCM_ID	SC_TIME [UTC]	Speed Increase [m/s]	Injection length [sec]	Remarks
TCM1_MZ	01:00:33	0.0038	0.065	Planned Value (TIMEREQ, 2 injections)
		0.00377		Doppler Measurments
		0.0037		ACM Integral Value

Accuracy DVZ 0.00377/0.0038 = 99.21%

DVZ 0.00377-0.0038 = -0.00003

Fig. 14: Results of the TCM1 operation on 2018/11/30: planned and measured ΔV report.

6.3 Deep Conjunction Epoch: 2018/12/11

During deep conjunction on the 2018/12/11, we performed beacon operations to test the Ka-band capability and the state vector of Hayabusa2 spacecraft was estimated [10]. Figure 15 shows in gray the propagated trajectory after estimating the state vector on 2018/12/11. Compared to the propagated trajectory after executing the actual ΔV at TCM1, we noticed a displacement in position of 2 km in the X-HP direction at TCM2. We believe that the 0.5 mm/s correction we didn't give at TCM1 in the X-axis is one of the causes of this expected position displacement at TCM2. Moreover, the trajectory designed between TCM1 and TCM2 with the optNEAR tool assumed that the spacecraft was always Earth-pointing. However, attitude maneuvers were given every 3 days that it resulted in an error in the pointing accuracy of 1° with a consequent less strong effect in the SRP acceleration. A lower effect in the SRP acceleration causes a drift in the x-axis direction away from the asteroid. We verified that by propagating the planned trajectory with a reflectively coefficient, C_r, 5% less than the nominal value would have compensated the error in the X-HP position. It is also possible that after 21 days the effect of non-linearities affected our solution therefore a TCM2 maneuver was needed right after deep conjunction on 2012/12/25.

The error in the attitude is also thought to be the reason why on 2018/12/15-17 the asteroid was not in the FOV of the ONC-T camera as shown in Fig 17. Figure 18 shows the angle between Ryugu and the spacecraft for each day after 2018/12/11 as one can see, when the error of 1° in the attitude is included in the analysis, Ryugu is not in the FOV of the ONC-T both days.

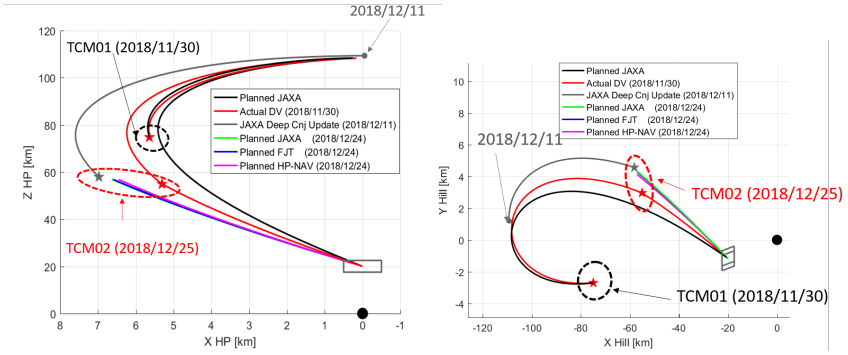

(a) X-Z HP view. (b) X-Y HP view.

Fig. 15: Estimated trajectory in deep conjunction after beacon operation.

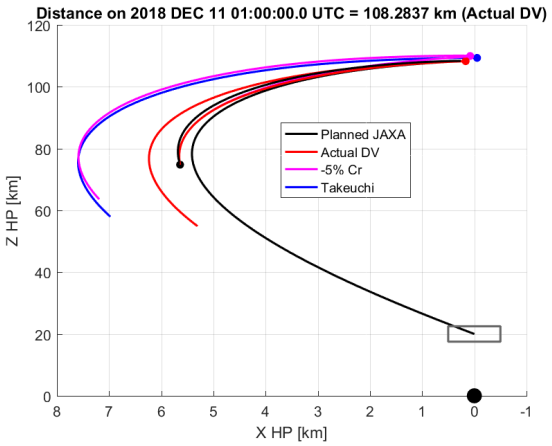

Fig. 16: Estimating the equivalent error in C_r.

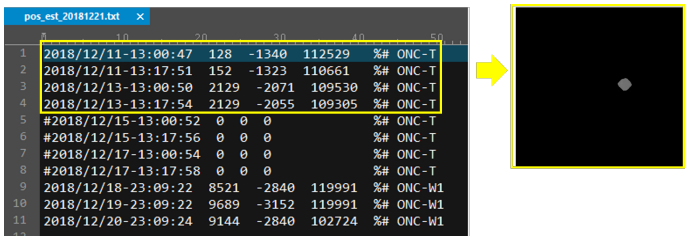

(a) Epoch 2018/12/11-13.

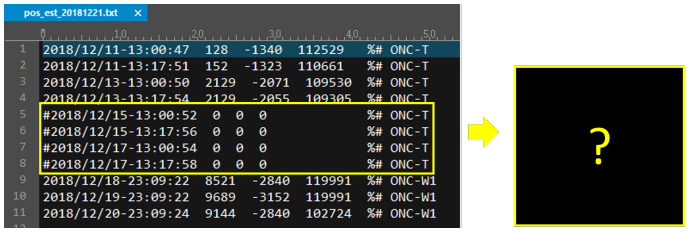

(b) Epoch 2018/12/15-17.

Fig. 17: Post estimation 2018/12/21: ONC-T images.

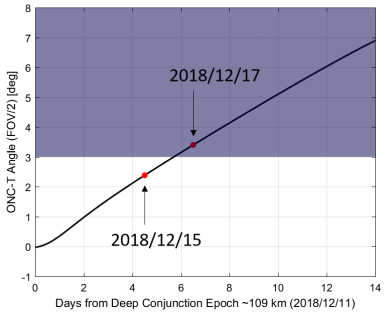

(a) No error in attitude.

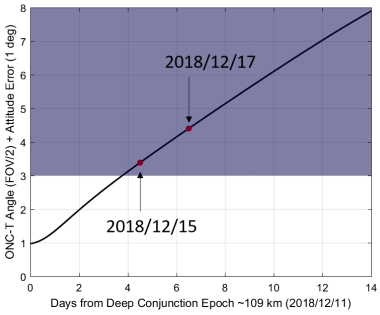

(b) Attitude error.

Fig. 18: ONC-T angle FOV as function of the days form deep conjunction: the blue area display at which epochs Ryugu is not in the FOV of ONC-T.

The observation campaign was started on the 2018/12/21 to verify that the Z-HP altitude was within the expected values. From the Doppler signal in Fig 19, we verified that the spacecraft's velocity has changed sign and that the spacecraft was returning to lower altitudes. The altitude of the spacecraft was, as planned, around 82 km and it was decreasing towards the HP position altitude.

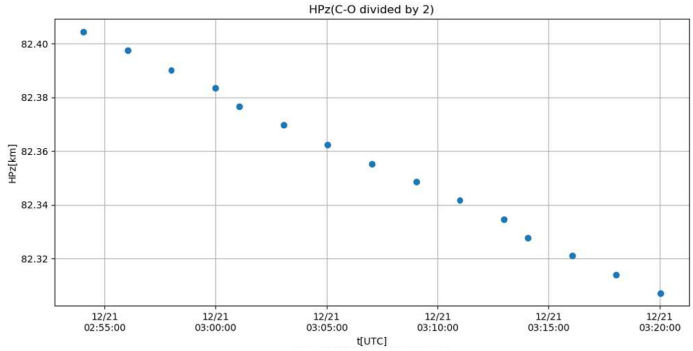

(a) Position.

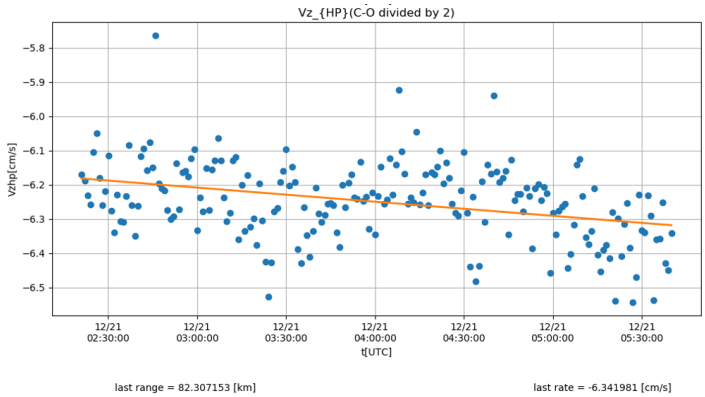

(b) Velocity.

Fig. 19: Doppler measurements on 2018/12/21.

6.4 Trajectory Correction Maneuver 2 (TCM2): 2018/12/25

After 21 days of blackout in the communication link, the first telemetry data from the spacecraft was downloaded on the 22^{nd} of December 2018. The second TCM2 maneuver was scheduled for the 25^{th} of December after the planning on Christmas eve.

(a) The estimates of the spacecraft's position and velocity on the 24^{th} of December are shown in Tab (8). As for the COI and TCM1 operations planning, the solutions are crosschecked with the nominal case designed after the TCM1 maneuver (green trajectory in Fig. 13) was executed. The ΔVs correspondent to the estimate solutions are shown in Tab (9). The ΔVs in Tab (9) are cross evaluated with the different solutions in Tab (8) and the solutions are propagated with goNEAR. From this analysis, the solution from Fujitsu was selected for the ΔV planning at TCM2.

Table 8: Nominal state vector at TCM2 and estimate states by Fujitsu (OPNAV1/NAV3 in Fig 3), JAXA (OPNAV2/NAV3 in Fig 3) and HPNAV (NAV1 in Fig 3).

State Estimate	x_{hp} [km]	y_{hp} [km]	z_{hp} [km]	$v_{x_{hp}}$ [mm/s]	$v_{y_{hp}}$ [mm/s]	$v_{z_{hp}}$ [mm/s]
Nominal	5.3185	-1.2411	55.0592	-0.6931	0.2238	-8.8516
OD's Fujitsu	6.6334	-1.8447	56.8919	-0.6281	0.1917	-8.6760
OD's JAXA	6.5968	-1.8250	56.8739	-0.6252	0.1940	-8.6823
HPNAV	6.4577	-1.7198	56.8581	-0.8764	0.2514	-8.7487

Table 9: Nominal ΔV, OD's Fujitsu ΔV (OPNAV1/NAV3 in Fig 3) and OD's JAXA ΔV (OPNAV2/NAV3 in Fig 3).

State Estimate	$\Delta\mathrm{VX}_{HP}$ [cm/s]	$\Delta\mathrm{VY}_{HP}$ [cm/s]	$\Delta\mathrm{VZ}_{HP}$ [cm/s]
Nominal	-3.0005	0.5207	1.5554
OD's Fujitsu	-7.0870	2.6334	-5.8566
OD's JAXA	-7.0163	2.5521	-5.7345

(b) Figure 20 shows the way file prepared on the 24^{th} of December for the TCM2 operation (2018/12/25). The OD's Fujitsu team way file is the input for the AOCS team and the ΔV is computed in body-fixed frame.

```
#OBJ_SIGMA -1.000000 OPTIMIZE_INISTATE 0
#DVNUM
 2
#=============================================================================================================================|
#.      TDB                UTC             X_HP      Y_HP      Z_HP      VX_HP     VY_HP     VZ_HP      DVX_HP      DVY_HP      DVZ_HP   |
#     [day]                                 [km]      [km]      [km]      [m/s]     [m/s]     [m/s]       [m/s]       [m/s]       [m/s]   |
#1------2-----------------3--------------4--------5--------6---------7--------8--------9---------10---------11---------12----|
 0  58476.875801 2018/12/24T21:00:00.0   6.7103  -1.8684  57.9790  -0.0059   0.0019  -0.0858  --------   --------    --------
 1  58477.021634 2018/12/25T00:30:00.0   6.6334  -1.8447  56.8919  -0.0134   0.0046  -0.0926   -0.0071    0.0026    -0.0059
 2  58481.028579 2018/12/29T00:40:00.0  -0.0002  -0.0000  20.0001   0.0001   0.0000   0.0134    0.0256    -0.0062     0.1367
 3  58483.209134 2018/12/31T05:00:00.0  -0.0001   0.0001  20.0000  -0.0004   0.0000  -0.0134  --------   --------    --------

#TOTAL DV
#=============================================================================================
#  dVTotal   dVx      dVy      dVz
#  [m/s]    [m/s]    [m/s]    [m/s]
#---1--------2--------3--------4-----------------------------------------------------------------
   0.1466  ------   ------   ------   #SUM OF dV NORM
   0.1841  0.0327   0.0088   0.1426   #SUM OF dVx,dVy,dVz
   0.2094  0.0327   0.0341   0.1426   #SUM OF FUEL-EQUIV dVx,dVy,dVz (ATT ALGN. if dVy>0.10[m/s])
   0.2094  0.0327   0.0341   0.1426   #SUM OF FUEL-EQUIV dVx,dVy,dVz (NO ATT ALGN.)
   0.0080  0.0018   0.0066   0.0042   #Stochastic DV 2.5-sigma(99%) [m/s]
```

Fig. 20: Planned ΔV at TCM2 in Way file format.

(c) As a consequence of cancelling the ΔVX,Y at TCM1, we performed the TCM2 in each X, Y and Z components, Fig 20. As expected the larger ΔV was given in the X direction as at TCM1, Fig. 11, we did not performed the $\Delta \mathrm{VX}_B$ of 0.5 mm/s that resulted in an expected 1 km displacement in X at TCM2. The error between the planned and the actual ΔV at TCM2 was of 105.89% in $\Delta \mathrm{VX}_B$, 100.21% in $\Delta \mathrm{VY}_B$ and 93.48% in $\Delta \mathrm{VZ}_B$ as shown in the report of Fig 21. Figure 22 shows the ayu trajectory displayed in the controlled room for the X-Z and Y-Z components in the HP frame at TCM2.

```
2018/12/25
================================================================================
TCM_ID   SC_TIME    Speed      Injection   Remarks
                    Increase   length
           [UTC]    [m/s]      [sec]
--------------------------------------------------------------------------------
TCM2_MX 00:35:33   -0.007206  -0.126      Planned Value
                   -0.007631              ACM Integral Value

TCM2_MZ 00:40:38   -0.005892  -0.113      Planned Value (TIMEREQ, 2 injections)
                   -0.005508              Doppler Measuments
                   -0.00702               ACM Integral Value

TCM2_MY 00:45:33    0.002310   0.147      Planned Value
                    0.002315              ACM Integral Value


--------------------------------------------------------------------------------
Accuracy   DVX      0.007631/0.007206  =  105.89%
           DVY      0.002315/0.002310  =  100.21%
           DVZ      0.005508/0.005892  =  93.48%

           DVX      0.007631-0.007206  =   0.000425
           DVY      0.002315-0.002310  =   0.000499
           DVZ      0.005508-0.005892  =  -0.00038
================================================================================
```

Fig. 21: Results of the TCM2 operation on 2018/12/25: planned and measured ΔV report.

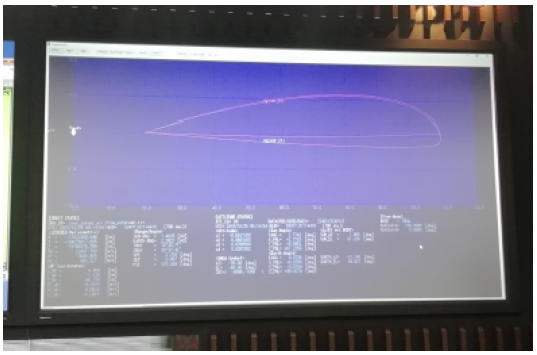

Fig. 22: Planned ayu trajectory displayed in the screen of the ISAS's control room on 2018/12/25.

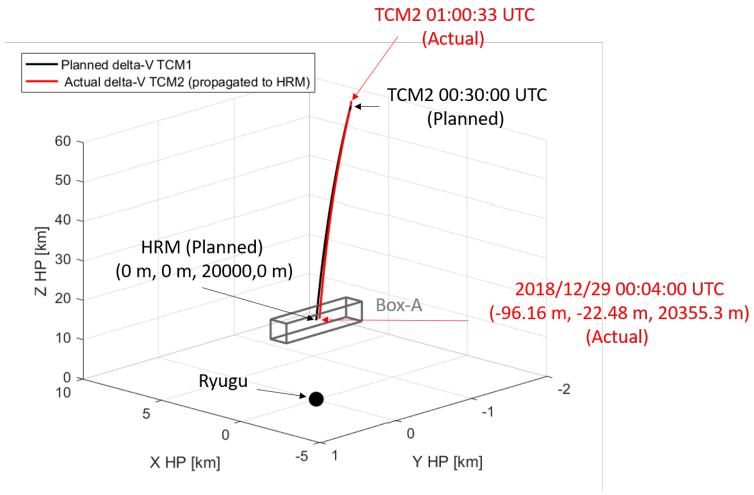

Fig. 23: Planned trajectory OD Fujitsu solution (black), actual trajectory after TCM2 operation (red) and BOX-A operation (gray). The black dot represents the Ryugu coordinates. HP reference frame.

6.5 Home Recovery Maneuver and Home Position Keeping: 2018/12/29

On the 29^{th} of December 2019, we performed the last conjunction operation. As explained in Section 4.3, we combined two ΔVs in one maneuver. We performed a Home Position Keeping (HPK) maneuver (BOX-A operation keeping until 2018/12/31) together with the HRM ΔV.

(a) Table (10) shows the estimates of the spacecraft's position and velocity on the 30^{th} of December. As for the previous operations, the solutions are crosschecked with the nominal case designed after the TCM2 maneuver (green trajectory in Fig. 23) was executed. The ΔVs correspondent to the

estimate solutions are shown in Tab (11). The ΔVs in Tab (11) are cross evaluated with the different solutions in Tab (10) and the solutions are propagated with goNEAR. From this analysis, the solution from Fujitsu was selected for the ΔV planning at HRM.

Table 10: Nominal state vector at HRM and estimate states by Fujitsu (OPNAV1/NAV3 in Fig 3), JAXA (OPNAV2/NAV3 in Fig 3) and HPNAV (NAV1 in Fig 3).

State Estimate	x_{hp} [km]	y_{hp} [km]	z_{hp} [km]	$v_{x_{hp}}$ [mm/s]	$v_{y_{hp}}$ [mm/s]	$v_{z_{hp}}$ [mm/s]
Nominal	-0.0993	-0.0217	20.3407	0.7	0.1	11.5
OD's Fujitsu	-0.6307	-0.0807	19.9176	3.3	0.4	14.0
OD's JAXA	-0.5825	-0.0923	19.7616	3.0	0.5	14.9
HPNAV	-0.6572	-0.0527	19.8053	3.4	0.3	14.6

Table 11: Nominal ΔV, OD's Fujitsu ΔV (OPNAV1/NAV3 in Fig 3) and OD's JAXA ΔV (OPNAV2/NAV3 in Fig 3).

State Estimate	$\Delta\mathrm{VX}_{HP}$ [cm/s]	$\Delta\mathrm{VY}_{HP}$ [cm/s]	$\Delta\mathrm{VZ}_{HP}$ [cm/s]
Nominal	0.2650	-0.0610	1.3410
OD's Fujitsu	0.3090	-0.0560	1.3750
OD's JAXA	0.3020	-0.0550	1.3800

(b) Figure 24 shows the way file prepared on the 30^{th} of December for the combined HRM and HPK maneuvers (2018/12/31). The OD's Fujitsu team way file is the input for the AOCS team and the ΔV is computed in body-fixed frame.

```
#OBJ_SIGMA -1.000000 OPTIMIZE_INISTATE 0
#DVNUM
 1
#=============================================================================================================================|
#.     TDB                UTC             X_HP     Y_HP     Z_HP     VX_HP    VY_HP    VZ_HP     DVX_HP     DVY_HP     DVZ_HP  |
#     [day]                                [km]     [km]     [km]     [m/s]    [m/s]    [m/s]      [m/s]      [m/s]      [m/s]  |
#1------2-----------------3---------------4--------5--------6---------7--------8--------9----------10---------11---------12----|
 0  58480.875801 2018/12/28T21:00:00.0  -0.2693  -0.1595  21.5371  -0.0271   0.0059  -0.1218  --------   --------    --------
 1  58481.028579 2018/12/29T00:40:00.0  -0.6307  -0.0807  19.9176   0.0033   0.0004   0.0140    0.0309    -0.0056     0.1375--
 2  58483.209134 2018/12/31T05:00:00.0  -0.0001   0.0001  19.9999   0.0031   0.0005  -0.0131  --------   --------    --------

#TOTAL DV
#=========================================================================================
#  dVTotal   dVx      dVy      dVz
#  [m/s]    [m/s]    [m/s]    [m/s]
#---1--------2--------3--------4-----------------------------------------------------------
   0.1411  ------   ------   ------   #SUM OF dV NORM
   0.1741  0.0309   0.0056   0.1375   #SUM OF dVx,dVy,dVz
   0.1901  0.0309   0.0217   0.1375   #SUM OF FUEL-EQUIV dVx,dVy,dVz (ATT ALGN. if dVy>0.10[m/s])
   0.1901  0.0309   0.0217   0.1375   #SUM OF FUEL-EQUIV dVx,dVy,dVz (NO ATT ALGN.)
   0.0000  0.0000   0.0000   0.0000   #Stochastic DV 2.5-sigma(99%) [m/s]
```

Fig. 24: Planned ΔV at HRM (including HPK) in Way file format.

(c) The HRM ΔV accounts of the brake velocity ΔV at HRM plus the Home Position Keeping (HPK) ΔV to target the center of BOX-A operation on 2018/12/31. We experienced a lower ΔV execution of 3 mm/s in both X and Y that allowed the braking velocity in the Z direction but not in the lateral direction.

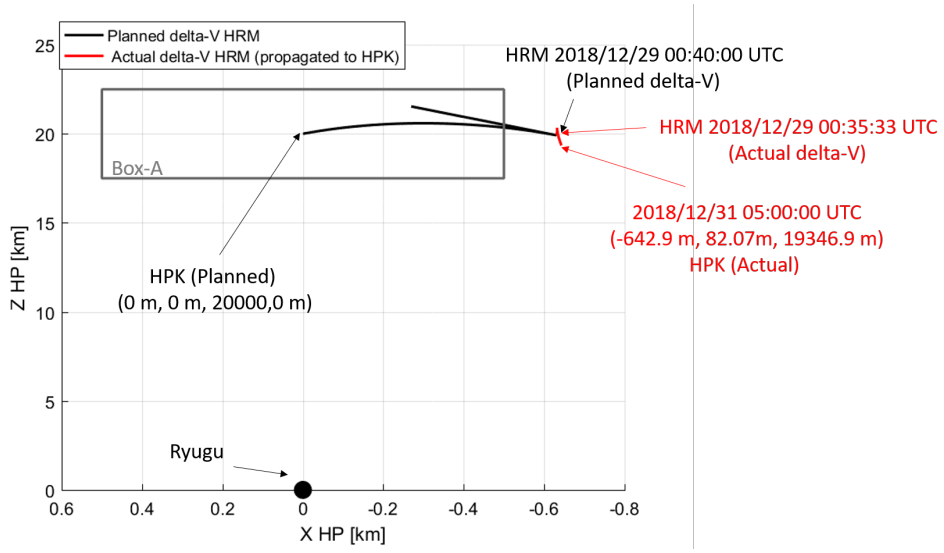

Fig. 25: Planned trajectory OD Fujitsu solution (black) and the actual trajectory after HRM operation (red). The edges of BOX-A are marked in gray. The black dot represents the Ryugu coordinates. HP reference frame.

The reason for a lower ΔV given is due to a decrease in the pressure in the fuel tank that had to be adjusted after the conjunction operation. The error between the planned and the actual ΔV at HRM was of 89.29% in ΔVX_B, 92.15% in ΔVY_B and 97.43% in ΔVZ_B as shown in the report of Fig 26. Therefore, on 2018/12/31 a BOX-A operation was performed to bring the spacecraft back to 20 km. The 2018/12/29 marked the end of the superior solar conjunction phase and the start of the second half of the Ryugu proximity operations.

2018/12/29

TCM_ID	SC_TIME [UTC]	Speed Increase [m/s]	Injection length [sec]	Remarks	
HRM_MX	00:35:33	0.0311	0.483	Planned Value	
		0.0277		ACM Integral Value	
HRM_MZ	00:40:38	0.1000	1.503	Planned Value (TIMEREQ, 2 injections)	
		0.09337		Doppler Measuments	
		0.09308		ACM Integral Value	
HRM_MY	00:45:33	-0.0053	-0.319	Planned Value	
		-0.00488		ACM Integral Value	
HRM_TZ	02:05:33	0.0375	0.575	Planned Value (Initially, 2 injections)	
		0.0441	0.673	Planned Value (HRM_MZ Influence, 2 injections)	
		0.0406		Doppler Measuments	
		0.0409		ACM Integral Value	
Accuracy	DVX	0.0277/0.0311			= 89.29%
	DVY	0.00488/0.0053			= 92.15%
	DVZ	(0.09337 + 0.0406)/(0.1000+0.0375)			= 97.43%
	DVX	0.0277-0.0311			= -0.0034
	DVY	0.00488-0.0053			= -0.00042
	DVZ	(0.09337 + 0.0406)-(0.1000+0.0375)			= -0.003530

Fig. 26: Results of the HRM (including HPK) operation on 2018/12/29: planned and measured ΔV report.

6.6 Summary of the Solar Conjunction Operation

In this section, we showed the results of the COI (2018/11/23), TCM1 (2018/11/30), TCM2 (2018/12/25) and HRM (2018/12/29) operations. The deterministic ΔV is computed for each trajectory legs with the optNEAR tool. The comparison between the planned trajectory after the OD campaign and the actual

ΔV trajectory after the mission operation are shown for COI (Fig 10), TCM1 (Fig 13), TCM2 (Fig 23) and HRM (Fig 25). In Fig. 10,13, 23 and25, the trajectory in black is the planned trajectory while the one in red is the propagated trajectory after measuring the actual ΔV. The deterministic ΔV is computed with optNEAR in J2000EQ and than given in the HP and spacecraft's body-fixed reference frames as shown in Tab 12. As previously mentioned, ΔV lower than 1 mm/s are neglected while ΔV major than 10 cm/s are executed in two times as main and trim ΔVs as shown in Tab 13. Tab 13 shows also the effect of the truncation in the ΔV up to 4 digits for the ΔV command. As one can see, both TCM1 and TCM2 do not require a trim ΔV while the Z direction requires a main and a trim ΔVs for both COI and HRM. The planned trim ΔV is usually rescheduled during the mission operation to compensate in the error of the main ΔV. In Tab 13, the actual measurements are the ACMs for the X and Y ΔVs and 2-way Doppler for the Z ΔV.

Table 12: Designed Deterministic ΔV in HP and Body-Fixed Frames.

Maneuver	ΔVX_{HP}	ΔVY_{HP}	ΔVZ_{HP}	ΔVX_B	ΔVY_B	ΔVZ_B
COI [cm/s]	2.154758	-0.290556	14.049689	-2.071104	0.595609	14.052644
TCM1 [cm/s]	0.049176	0.004165	0.379261	-0.048507	0.005917	0.379325
TCM2 [cm/s]	-0.708705	0.263339	-0.585655	-0.719433	0.234432	-0.584859
HRM [cm/s]	3.092521	-0.560379	13.753272	3.111279	-0.530874	13.750199

Table 13: Planned and actual executed ΔV in the Body-Fixed Frame.

Maneuver	ΔVX_B (Planned)	ΔVY_B (Planned)	ΔVZ_B (Planned)	ΔVX_B (Actual)	ΔVY_B (Actual)	ΔVZ_B (Actual)
COI (Main) [cm/s]	-2.0700	0.5900	10.0000	-2.0448	0.54918	9.4530
COI (Trim) [cm/s]	0.0000	0.0000	4.5970	0.0000	0.0000	4.3900
TCM1 (Main) [cm/s]	0.0000	0.0000	0.3800	0.0000	0.0000	0.3770
TCM1 (Trim) [cm/s]	0.0000	0.0000	0.0000	0.0000	0.0000	0.0000
TCM2 (Main) [cm/s]	-0.7206	0.2310	-0.5892	-0.7631	0.2315	-0.5508
TCM2 (Trim) [cm/s]	0.0000	0.0000	0.0000	0.0000	0.0000	0.0000
HRM (Main) [cm/s]	3.0900	-0.5600	10.0000	2.7700	-0.4880	9.3370
HRM (Trim) [cm/s]	0.0000	0.0000	4.4100	0.0000	0.0000	4.0600

7 Conclusion

In this article, we presented the flown Hayabusa2's low energy conjunction (ayu) trajectory executed in late 2018. As a result of the operation, the opt-NEAR tool was validated in real time and it was used for the validation of JAXA's JATOPS trajectory design tool at high altitude operations. The spacecraft reached a maximum distance of 109 km from Ryugu on December 11,

2018 and it returned at Home Position (20 km distance from Ryugu) on December 29, 2018 after 21 days of uncontrolled orbital motion. Due to the error in the attitude maintenance in deep conjunction, Ryugu was not in the FOV of the ONC-T camera on the 2019/12/15 while it was always in the FOV of ONC-W1. On 2018/12/11 (Deep conjunction), a beacon operation was performed for radio science purposes to test the Ka-band capability under the solar corona noise. The total expenditure in the ΔV was, as desired, less than 0.36 m/s. Based on the observation data collected during the solar conjunction, we recalculated the orbit of the asteroid Ryugu. This updated orbit was used after returning to HP position (HRM) to resume the home position at an altitude of 20 km above the asteroid surface. We were able to confirm that by using this new orbit of Ryugu a more stable maintenance of the home position can now be achieved.

Appendix A: Partial Derivatives of the optNEAR's Linearised Equations

The partial derivatives including the gravity of Ryugu, the 3^{rd} body and the SRB perturbations are given by the following equation:

$$\begin{bmatrix} \frac{\partial F_4}{\partial x} & \frac{\partial F_4}{\partial y} & \frac{\partial F_4}{\partial z} \\ \frac{\partial F_5}{\partial x} & \frac{\partial F_5}{\partial y} & \frac{\partial F_5}{\partial z} \\ \frac{\partial F_6}{\partial x} & \frac{\partial F_6}{\partial y} & \frac{\partial F_6}{\partial z} \end{bmatrix} = \begin{bmatrix} \frac{\partial F_{4r}}{\partial x} & \frac{\partial F_{4r}}{\partial y} & \frac{\partial F_{4r}}{\partial z} \\ \frac{\partial F_{5r}}{\partial x} & \frac{\partial F_{5r}}{\partial y} & \frac{\partial F_{5r}}{\partial z} \\ \frac{\partial F_{6r}}{\partial x} & \frac{\partial F_{6r}}{\partial y} & \frac{\partial F_{6r}}{\partial z} \end{bmatrix} + \sum_{j=1}^{NP_j} \begin{bmatrix} \frac{\partial F_{4p_j}}{\partial x} & \frac{\partial F_{4p_j}}{\partial y} & \frac{\partial F_{4p_j}}{\partial z} \\ \frac{\partial F_{5p_j}}{\partial x} & \frac{\partial F_{5p_j}}{\partial y} & \frac{\partial F_{5p_j}}{\partial z} \\ \frac{\partial F_{6p_j}}{\partial x} & \frac{\partial F_{6p_j}}{\partial y} & \frac{\partial F_{6p_j}}{\partial z} \end{bmatrix} + \begin{bmatrix} \frac{\partial F_{4srp}}{\partial x} & \frac{\partial F_{4srp}}{\partial y} & \frac{\partial F_{4srp}}{\partial z} \\ \frac{\partial F_{5srp}}{\partial x} & \frac{\partial F_{5srp}}{\partial y} & \frac{\partial F_{5srp}}{\partial z} \\ \frac{\partial F_{6srp}}{\partial x} & \frac{\partial F_{6srp}}{\partial y} & \frac{\partial F_{6srp}}{\partial z} \end{bmatrix} \tag{21}$$

7.1 Partial Derivatives of the Ryugu's Gravity

The partial derivatives of the Ryugu's gravity are given by:

$$\begin{bmatrix} \frac{\partial F_{4r}}{\partial x} & \frac{\partial F_{4r}}{\partial y} & \frac{\partial F_{4r}}{\partial z} \\ \frac{\partial F_{5r}}{\partial x} & \frac{\partial F_{5r}}{\partial y} & \frac{\partial F_{5r}}{\partial z} \\ \frac{\partial F_{6r}}{\partial x} & \frac{\partial F_{6r}}{\partial y} & \frac{\partial F_{6r}}{\partial z} \end{bmatrix} = \begin{bmatrix} -\frac{\mu_a}{r^3}\left[1-\frac{3x^2}{r^2}\right] & \mu_a\frac{3xy}{r^5} & \mu_a\frac{3xz}{r^5} \\ \mu_a\frac{3xy}{r^5} & -\frac{\mu_a}{r^3}\left[1-\frac{3y^2}{r^2}\right] & \mu_a\frac{3yz}{r^5} \\ \mu_a\frac{3xz}{r^5} & \mu_a\frac{3yz}{r^5} & -\frac{\mu_a}{r^3}\left[1-\frac{3z^2}{r^2}\right] \end{bmatrix} \tag{22}$$

7.2 Partial Derivatives of the 3^{rd} Body Perturbations

The partial derivatives of the 3^{rd} Body Perturbation are derived as:

$$\begin{bmatrix} \frac{\partial F_{4_{P_j}}}{\partial x} & \frac{\partial F_{4_{P_j}}}{\partial y} & \frac{\partial F_{4_{P_j}}}{\partial z} \\ \frac{\partial F_{5_{P_j}}}{\partial x} & \frac{\partial F_{5_{P_j}}}{\partial y} & \frac{\partial F_{5_{P_j}}}{\partial z} \\ \frac{\partial F_{6_{P_j}}}{\partial x} & \frac{\partial F_{6_{P_j}}}{\partial y} & \frac{\partial F_{6_{P_j}}}{\partial z} \end{bmatrix} = \begin{bmatrix} -\frac{\mu_{Pj}}{\Delta^3}\left[1-\frac{3(x-d_x)^2}{\Delta^2}\right] & \mu_{Pj}\frac{3(x-d_x)(y-d_y)}{\Delta^5} & \mu_{Pj}\frac{3(x-d_x)(z-d_z)}{\Delta^5} \\ \mu_{Pj}\frac{3(x-d_x)(y-d_y)}{\Delta^5} & -\frac{\mu_{Pj}}{\Delta^3}\left[1-\frac{3(y-d_y)^2}{\Delta^2}\right] & \mu_{Pj}\frac{3(y-d_z)(z-d_z)}{\Delta^5} \\ \mu_{Pj}\frac{3(x-d_x)(z-d_z)}{\Delta^5} & \mu_{Pj}\frac{3(y-d_y)(z-d_z)}{\Delta^5} & -\frac{\mu_{Pj}}{\Delta^3}\left[1-\frac{3(z-d_z)^2}{\Delta^2}\right] \end{bmatrix} \tag{23}$$

7.3 Partial Derivatives of Solar Radiation Pressure Perturbation

The cannonball model assumes that the Hayabusa2's spacecraft is Sun-pointing. This is not exact during the conjunction phase where Hayabusa2 is kept Earth-pointing. Therefore, the equation for a flat surface are more appropriate and used here. The partial derivatives of Eq. (4) are given by rearranging Eq. (4) as follow:

$$\boldsymbol{a}_{SRP} = -\frac{K(1-\epsilon)}{r_{Earth}}\frac{\boldsymbol{r}_{Earth}\cdot\boldsymbol{r}_{ls}}{r_{ls}^4}\boldsymbol{r}_{ls} - \frac{2K\epsilon}{r_{Earth}^3}\frac{(\boldsymbol{r}_{Earth}\cdot\boldsymbol{r}_{ls})^2}{r_{ls}^4}\boldsymbol{r}_{Earth}, \tag{24}$$

with K:

$$K = \frac{P_0}{c}\frac{A}{m}AU^2. \tag{25}$$

Note that:

$$\boldsymbol{r}_{Earth} = \begin{Bmatrix} X_E \\ Y_E \\ Z_E \end{Bmatrix} \qquad and \qquad \boldsymbol{r}_{ls} = \begin{Bmatrix} X_S - X \\ Y_S - Y \\ Z_S - Z \end{Bmatrix} \tag{26}$$

The derivatives of the two terms in Eq. (24) are derived by components and we distinguished between the 1^{st} term of Eq. (24) and 2^{nd} term of Eq. (24). The partial derivatives of SRP are:

$$\begin{bmatrix} \frac{\partial F_{4srp}}{\partial x} & \frac{\partial F_{4srp}}{\partial y} & \frac{\partial F_{4srp}}{\partial z} \\ \frac{\partial F_{5srp}}{\partial x} & \frac{\partial F_{5srp}}{\partial y} & \frac{\partial F_{5srp}}{\partial z} \\ \frac{\partial F_{6srp}}{\partial x} & \frac{\partial F_{6srp}}{\partial y} & \frac{\partial F_{6srp}}{\partial z} \end{bmatrix} = -\frac{K(1-\epsilon)}{r_{Earth}}\begin{bmatrix} a_{1xx} & a_{1xy} & a_{1xz} \\ a_{1yx} & a_{1yy} & a_{1yz} \\ a_{1zx} & a_{1zy} & a_{1zz} \end{bmatrix} - \frac{2K\epsilon}{r_{Earth}^3}\begin{bmatrix} a_{2xx} & a_{2xy} & a_{2xz} \\ a_{2yx} & a_{2yy} & a_{2yz} \\ a_{2zx} & a_{2zy} & a_{2zz} \end{bmatrix} \tag{27}$$

This formulation was written for a flat surface Earth-pointing, therefore the norm is function of Earth-Asteroid line for simplicity. The two terms of Eq. (27) are derived by components as:

1) **1^{st} Term**

$$\frac{\boldsymbol{r}_{Earth}\cdot\boldsymbol{r}_{ls}}{r_{ls}^4}\boldsymbol{r}_{ls} = \frac{X_E(X_S-X)+Y_E(Y_S-Y)+Z_E(Z_S-Z)}{\left((X_S-X)^2+(Y_S-Y)^2+(Z_S-Z)^2\right)^2}\begin{Bmatrix} X_S-X \\ Y_S-Y \\ Z_S-Z \end{Bmatrix} = \boldsymbol{a}_1 \tag{28}$$

Derivatives of the x-component

$$\frac{\partial a_{1x}}{\partial x} = a_{1xx} = -\frac{2X_E(X_S - X) + Y_E(Y_S - Y) + Z_E(Z_S - Z)}{r_{ls}^4} + 4\frac{\boldsymbol{r}_{Earth} \cdot \boldsymbol{r}_{ls}(X_S - X)^2}{r_{ls}^6} \tag{29}$$

$$\frac{\partial a_{1x}}{\partial y} = a_{1xy} = -\frac{Y_E(X_S - X)}{r_{ls}^4} + 4\frac{\boldsymbol{r}_{Earth} \cdot \boldsymbol{r}_{ls}(X_S - X)(Y_S - Y)}{r_{ls}^6} \tag{30}$$

$$\frac{\partial a_{1x}}{\partial z} = a_{1xz} = -\frac{Z_E(X_S - X)}{r_{ls}^4} + 4\frac{\boldsymbol{r}_{Earth} \cdot \boldsymbol{r}_{ls}(X_S - X)(Z_S - Z)}{r_{ls}^6} \tag{31}$$

Derivative of the y-component

$$\frac{\partial a_{1y}}{\partial x} = a_{1yx} = -\frac{X_E(Y_S - Y)}{r_{ls}^4} + 4\frac{\boldsymbol{r}_{Earth} \cdot \boldsymbol{r}_{ls}(Y_S - Y)(X_S - X)}{r_{ls}^6} \tag{32}$$

$$\frac{\partial a_{1y}}{\partial y} = a_{1yy} = -\frac{X_E(X_S - X) + 2Y_E(Y_S - Y) + Z_E(Z_S - Z)}{r_{ls}^4} + 4\frac{\boldsymbol{r}_{Earth} \cdot \boldsymbol{r}_{ls}(Y_S - Y)^2}{r_{ls}^6} \tag{33}$$

$$\frac{\partial a_{1y}}{\partial z} = a_{1yz} = -\frac{Z_E(Y_S - Y)}{r_{ls}^4} + 4\frac{\boldsymbol{r}_{Earth} \cdot \boldsymbol{r}_{ls}(Y_S - Y)(Z_S - Z)}{r_{ls}^6} \tag{34}$$

Derivative of the z-component

$$\frac{\partial a_{1z}}{\partial x} = a_{1zx} = -\frac{X_E(Z_S - Z)}{r_{ls}^4} + 4\frac{\boldsymbol{r}_{Earth} \cdot \boldsymbol{r}_{ls}(Z_S - Z)(X_S - X)}{r_{ls}^6} \tag{35}$$

$$\frac{\partial a_{1z}}{\partial y} = a_{1zy} = -\frac{Y_E(Z_S - Z)}{r_{ls}^4} + 4\frac{\boldsymbol{r}_{Earth} \cdot \boldsymbol{r}_{ls}(Z_S - Z)(Y_S - Y)}{r_{ls}^6} \tag{36}$$

$$\frac{\partial a_{1z}}{\partial z} = a_{1zz} = -\frac{X_E(X_S - X) + Y_E(Y_S - Y) + 2Z_E(Z_S - Z)}{r_{ls}^4} + 4\frac{\boldsymbol{r}_{Earth} \cdot \boldsymbol{r}_{ls}(Z_S - Z)^2}{r_{ls}^6} \tag{37}$$

2) **2^{nd} Term**

$$\frac{(\boldsymbol{r}_{Earth} \cdot \boldsymbol{r}_{ls})^2}{r_{ls}^4}\boldsymbol{r}_{Earth} = \frac{(X_E(X_S - X) + Y_E(Y_S - Y) + Z_E(Z_S - Z))^2}{\left((X_S - X)^2 + (Y_S - Y)^2 + (Z_S - Z)^2\right)^2} \begin{Bmatrix} X_E \\ Y_E \\ Z_E \end{Bmatrix} = \boldsymbol{a}_2 \tag{38}$$

Partial derivatives of

$$\frac{\partial}{\partial \boldsymbol{r}} \frac{(\boldsymbol{r}_{Earth} \cdot \boldsymbol{r}_{ls})^2}{r_{ls}^4} = 2\frac{\boldsymbol{r}_{Earth} \cdot \boldsymbol{r}_{ls}}{r_{ls}^4} \frac{\partial(\boldsymbol{r}_{Earth} \cdot \boldsymbol{r}_{ls})}{\partial \boldsymbol{r}} - \frac{(\boldsymbol{r}_{Earth} \cdot \boldsymbol{r}_{ls})^2}{r_{ls}^8} \frac{\partial r_{ls}^4}{\partial \boldsymbol{r}} \tag{39}$$

where

$$\frac{\partial(\boldsymbol{r}_{Earth} \cdot \boldsymbol{r}_{ls})}{\partial \boldsymbol{r}} = -\begin{Bmatrix} X_E \\ Y_E \\ Z_E \end{Bmatrix} \tag{40}$$

and

$$\frac{\partial r_{ls}^4}{\partial \boldsymbol{r}} = -4\left((X_S - X)^2 + (Y_S - Y)^2 + (Z_S - Z)^2\right)\begin{Bmatrix} X_S - X \\ Y_S - Y \\ Z_S - Z \end{Bmatrix} \tag{41}$$

therefore

$$\frac{\partial}{\partial \boldsymbol{r}} \frac{(\boldsymbol{r}_{Earth} \cdot \boldsymbol{r}_{ls})^2}{r_{ls}^4} = -2\frac{\boldsymbol{r}_{Earth} \cdot \boldsymbol{r}_{ls}}{r_{ls}^4}\begin{Bmatrix} X_E \\ Y_E \\ Z_E \end{Bmatrix} + 4\frac{(\boldsymbol{r}_{Earth} \cdot \boldsymbol{r}_{ls})^2}{r_{ls}^6}\begin{Bmatrix} X_S - X \\ Y_S - Y \\ Z_S - Z \end{Bmatrix} \tag{42}$$

Finally

$$\begin{bmatrix} a_{2xx} & a_{2xy} & a_{2xz} \\ a_{2yx} & a_{2yy} & a_{2yz} \\ a_{2zx} & a_{2zy} & a_{2zz} \end{bmatrix} = \left[-2\frac{\boldsymbol{r}_{Earth} \cdot \boldsymbol{r}_{ls}}{r_{ls}^4}\begin{Bmatrix} X_E \\ Y_E \\ Z_E \end{Bmatrix} + 4\frac{(\boldsymbol{r}_{Earth} \cdot \boldsymbol{r}_{ls})^2}{r_{ls}^6}\begin{Bmatrix} X_S - X \\ Y_S - Y \\ Z_S - Z \end{Bmatrix}\right]\begin{bmatrix} X_E & Y_E & Z_E \end{bmatrix} \tag{43}$$

7.4 Partial Derivatives of Solar Radiation Pressure Perturbation (Sun-Pointing)

For a cannonball model, the partial derivatives of the SRP perturbation are quite simple and they are given by:

$$\begin{bmatrix} \frac{\partial F_{4srp}}{\partial x} & \frac{\partial F_{4srp}}{\partial y} & \frac{\partial F_{4srp}}{\partial z} \\ \frac{\partial F_{5srp}}{\partial x} & \frac{\partial F_{5srp}}{\partial y} & \frac{\partial F_{5srp}}{\partial z} \\ \frac{\partial F_{6srp}}{\partial x} & \frac{\partial F_{6srp}}{\partial y} & \frac{\partial F_{6srp}}{\partial z} \end{bmatrix} = \begin{bmatrix} \frac{K}{r^3}\left[1 - \frac{3x^2}{r^2}\right] & -K\frac{3xy}{r^5} & -K\frac{3xz}{r^5} \\ -K\frac{3xy}{r^5} & \frac{K}{r^3}\left[1 - \frac{3y^2}{r^2}\right] & -K\frac{3yz}{r^5} \\ -K\frac{3xz}{r^5} & -K\frac{3yz}{r^5} & \frac{K}{r^3}\left[1 - \frac{3z^2}{r^2}\right] \end{bmatrix}, \tag{44}$$

with K:

$$K = \frac{P_0 C_r}{c}\frac{A_{sc}}{m_{sc}} AU^2. \tag{45}$$

References

1. Belbruno, E., Miller, A.: A balistic lunar capture trajectory for the japanese spacecraft hiten. Jet Propulsion Laboratory, IOM 312/90.41371-EAB (1990)
2. Koon, W.S., Lo, M.W., Marsden, J.E., Ross, S.D.: Dynamical Systems, the Three-Body Problem and Space Mission Design. Caltech (2006)
3. Lauretta, D., Balram-Knutson, S., Beshore, E., Boynton, W., dAubigny, C., DellaGiustina, D., Enos, H., Gholish, D., Hergenrother, C., Howell, E., Johnson, C., Morton, E., Nolan, M., Rizk, B., Roper, H., Bartels, A., Bos, B., Dworkin, J., Highsmith, D., Sandford, S.: Osiris-rex: Sample return from asteroid (101955) bennu. Space Science Reviews (2017). DOI 10.1007/s11214-017-0405-1
4. Montenbruck, O., Gill, E.: Satellite Orbits Model, Methods and Applications. Springer (2005)
5. Morley, T., Budnik, F.: Effects on spacecraft radiometric data at superior solar conjunction. 20^{th} International Symposium on Space Flight Dynamics, 24-28, September, Annapolis, United States **ISSFD** (2007)
6. Ono, G., Tsuda, Y., Akatsuka, K., Saiki, T., Mimasu, Y., Ogawa, N., Terui, F.: Generalized attitude model for momentum-biased solar sail spacecraft. Journal of Guidance, Control, and Dynamics **39**(7), 1491–1500 (2016). DOI 10.2514/1.G001750
7. Soldini, S., Takanao, S., Ikeda, H., Wada, K., Yuichi, T., Hirata, N., Hirata, N.: A generalised methodology for analytic construction of 1:1 resonances around irregular bodies: Application to the asteroid ryugu's ejecta dynamics. Planetary and Space Science p. 104740 (2019). DOI 10.1016/j.pss.2019.104740
8. Soldini, S., Yamaguchi, T., Tsuda, Y., Saiki, T.: Hayabusa2's superior solar conjunction phase for hovering satellite. In Preparation
9. Soldini, S., Yamaguchi, T., Tsuda, Y., Saiki, T.: Hayabusa2 mission solar conjunction trajectory for hovering satellite: Design, navigation and post-operation evaluation. 29^{th} AAS/AIAA Space Flight Mechanics Meeting **AAS 19-241** (January 13-17 Maui, HI)
10. Takeuchi, H.: The deepspace multi-objects orbit determination system and its application to hayabusa2's asteroid proximity operations. Astrodynamics: Special Issue on Astrodynamics and Engineering Aspects of Hayabusa2 – Sample Return Mission to the Asteroid Ryugu (Under Review) (2020)
11. Tsuda, Y., Saiki, T., Funase, R., Mimasu, Y.: Generalized attitude model for spinning solar sail spacecraft. Journal of Guidance, Control, and Dynamics **36**(4), 967–974 (2013). DOI 10.2514/1.59516
12. Tsuda, Y., Takeuchi H.and Ogawa, N.O.G., Kikuchi, S., Oki, Y., Ishiguro, M., Kuroda, D., Urakawa, S., Okumura, S.: Guidance and navigation result of hayabusa2 asteroid rendezvous operation. 32^{nd} International Symposium on Space Technology and Science (ISTS), Fukui, Japan, 2019
13. Tsuda, Y., Yoshikawa, M., Abe, M., Minamino, H., Nakazawa, S.: System design of the hayabusa2 – asteroid sample return mission to 1999 ju3. Acta Astronautica (91), 356–362 (2013)
14. Uesugi, K., Matuso, H., Kawaguchi, J., Hayashi, T.: Japanese first double lunar swingby mission "hiten". Acta Astronautica **25**, 347–355 (1991). DOI 10.1016/0094-5765(91)90014-V
15. Watanabe, S., Hirabayashi, M., Hirata, N., Noguchi, R., Shimaki, Y., Ikeda, H., Tatsumi, E., Yoshikawa, M., Kikuchi, S., Yabuta, H., Nakamura, T., Tachibana, S., Ishihara, Y., Morota, T., Kitazato, K., Sakatani, N., Matsumoto, K., Wada, K., Senshu, H., Honda, C., Michikami, T., Takeuchi, H., Kouyama, T., Honda, R., Kameda, S., Fuse, T., Miyamoto, H., Komatsu, G., Sugita, S., Okada, T., Namiki, N., Arakawa, M., Ishiguro, M., Abe, M., Gaskell, R., Palmer, E., Barnouin, O.S., Michel, P., French, A.S., McMahon, J.W., Scheeres, D.J., Abell, P.A., Yamamoto, Y., Tanaka, S., Shirai, K., Matsuoka, M., Yamada, M., Yokota, Y., Suzuki, H., Yoshioka, K., Cho, Y., Tanaka, S., Nishikawa, N., Sugiyama, T., Kikuchi, H., Hemmi, R., Yamaguchi, T., Ogawa, N., Ono, G., Mimasu, Y., Yoshikawa, K., Takahashi, T., Takei, Y., Fujii, A., Hirose, C., Iwata, T., Hayakawa, M., Hosoda, S., O. Mori2, H.S., Shimada, T., Soldini, S., Yano, H., Tsukizaki, R., Ozaki, M., Iijima, Y., Ogawa, K., Fujimoto, M., Ho, T.M., Moussi, A., Jaumann, R., Bibring, J.P., Krause, C., Terui, F., Saiki, T., Nakazawa, S., Tsuda, Y.:

Hayabusa2 observations of the top-shape carbonaceous asteroid 162173 ryugu. Scienece **364**(6437), 268–272 (2019). DOI 10.1126/science.aav8032
16. Y. Tsuda G. Ono, T.S.Y.M.N.O.F.T.: Srp-assisted fuel-free sun tracking and its application to hayabusa2. Journal of Spacecraft and Rockets **54**(6), 1284–1293 (2017). DOI 10.2514/1.A33799
17. Yoshikawa, M., Yano, H., Kawaguchi, J., Fujiwara, A., Abe, M., Iwata, T., Tanaka, S., Mori, O., Yoshimitsu, T., Takagi, Y., Demura, H., Noguchi, T., Miyamoto, H.: Technologies for future asteroid exploration: What we learned from hayabusa mission. LPI Contributions p. 1325:81 (2013)